ANTI-LOCK BRAKE SYSTEM (ABS) via

SLIDING MODE CONTROL

by

BARAN BARIS

Submitted to the Graduate School of Engineering and Natural Sciences

in partial fulfillment of

the requirements for the degree of

Master of Science

Sabanci University

2008

ANTI-LOCK BRAKE SYSTEM (ABS) via
SLIDING MODE CONTROL

APPROVED BY

Prof. Dr. Asif SABANOVIC   ………………………..
(Thesis Supervisor)

Assoc. Prof. Dr. Mustafa UNEL   ………………………..

Assoc. Prof. Dr. Mahmut F. AKSIT   ………………………..

Assist. Prof. Dr. Ahmet ONAT   ………………………..

Assist. Prof. Dr. Hakan ERDOGAN   ………………………..

DATE OF APPROVAL: ……………………

Acknowledgements

First of all, I would like to thank to my thesis supervisor Prof. Asif Sabanovic for his attitude, invaluable guidance and support throughout my research.

I am also thankful to Assoc. Prof. Mustafa Unel for his efforts and unconditional support during the study.

Finally, my greatest thanks will go to my family, especially to my wife. Their support, trust and motivation I can't compare to anything else.

Abstract

In a conventional anti-lock brake system (ABS) the basic control algorithm is a combination of wheel acceleration/deceleration control and the wheel slip control. This control algorithm depends on the pre-configured threshold values that vary for each braking scenario which requires a large amount of field testing to achieve the best performance. In addition to that, the unpredictable nature of the driving conditions results in limitations not only in tracking the desired slip value within an acceptable range but also in the maximization of the friction force. In this work, a robust ABS algorithm based on Sliding Mode Control (SMC) technique is introduced. It is shown that regardless of uncertainties in the driving conditions the friction force is maximized and the stability of the vehicle is maintained resulting in a shorter brake distance and a better steer ability. For that purpose a self optimization method that calculates the desired slip value and a wheel slip controller to track this slip value are mainly proposed. Similar optimization methods and slip controllers based on SMC can be found in the literature, but these methods are only tested in the Matlab/Simulink environment. In this project the proposed system is analyzed and tested in a vehicle simulator to provide more realistic results. In addition to the optimization method a friction force controller to maintain the friction force balance between the wheels hence maintaining the vehicle stability is also proposed and tested.

Özet

Konvansiyonel kilitlenmeyen fren sistemlerinde (ABS) temel kontrol algoritması tekerlek ivme kontorlunun ve kayma kontrolunun bir kombinasyonudur. Bu kontrol algoritması sürüş koşullarına göre farklılık gösteren kayma ve ivme eşik değerlerinin önceden tanımlanmış olmasına gereksinim duyduğundan en iyi performansın alınabilmesi icin uzun saha testi sürecine gereksinim duyar. Bunun yanı sıra, sürüş koşullarındaki degişkenlik istenilen kayma degerinin istenilen sapma sınırları icerisindeki takibinde ve surtunme kuvvetinin maksimize edilmesinde sınırlayıcı bir etken oluşturur. Bu çalışmada, Kayma Kipli Kontrol (KKK) tekniği üzerine oturtulmuş dayanıklı bir ABS algoritması sunulmuştur. Sürüş koşullarından bağımsız olarak teker sürtünme kuvvetinin maksimize edilerek ve araç stabilitesi korunarak daha kısa duruş mesafesine ve direksiyon hakimiyetinin daha iyi olduğu frenlemeye ulaşıldığı gösterilmiştir. Bu amaçla, hedeflenen kayma değerini hesaplayan bir optimizasyon metodu, belirtilen kayma değerini takip eden bir teker kayma kontrol metodu önerilmiştir. KKK temelli benzer optimizasyon ve teker kayma metotları literatürde mevcuttur, yalnız bu metotlar sadece Matlab/Simulink ortamında test edilmiştir. Bu projede, daha gerçekçi sonuçlar elde edilmesi amacıyla, önerilen sistem analiz edilmiş ve bir sürüş simulatöründe test edilmiştir. Önerilen optimizasyon metotuna ek olarak teker sürtünme kuvvetleri arasındaki dengeyi koruyan bir surtunme kuvveti kontrol metodu önerilmiş ve test edilmiştir.

Table of Contents

List of Figures

Abbrevations

ABC: Active body control

ABS: Antilock brake system

ACC: Adaptive cruise control

CAN: Control Area Network

CoG: Center of Gravity

EBD: Electronic brakeforce distribution

ECU: Electronic control unit

EHB: Electrohydraulic brakes

ESP: Electronic stability program

ETC: Electronic traction control

PID: Proportional Integral Derivative

SAE: Society of Automotive Engineers

SMC: Sliding Mode Control

TCS: Traction control system

1 Introduction

An **anti-lock braking system (ABS)** is actually translated from German, ***antiblockiersystem***. The system allows the driver to maintain steering control under hard braking by preventing a skid and allowing the wheel to continue to forward roll and create lateral control, as directed by driver steering inputs. Most commonly, braking distances are shortened (again, by allowing the driver to press the brake pedal fully without skidding or loss of control).

The motivation for an anti-lock braking system (ABS) is that it can provide improvements in the performance of the vehicle under braking compared to a conventional brake system. Performance improvement is typically sought in the areas of stability, steer ability and stopping distance. An ABS controls the slip of each wheel to prevent it from locking such that a high friction is achieved and steer ability is maintained. ABS controllers are characterized by robust adaptive behavior with respect to highly uncertain tire characteristics and fast changing road surface properties (SAE, 1992) (Burckhardt, 1993).

This chapter gives an overview on ABS systems, followed by a literature review and the outline of this thesis.

1.1 ABS System Overview

The current hydraulic ABS systems were conceived from systems developed for trains in the early 1900's. Next, anti-lock brakes were developed to assist aircrafts stop straight and quickly on slippery runways. In 1947, the first use of anti-lock brakes on airplanes was on B-47 bombers to avoid tire blowout on dry concrete and spin-outs on icy runways. The first automotive use of ABS was in 1954 on a limited number of Lincolns which were fitted with an ABS from a French aircraft. In the late 60's, Ford, Chrysler, and Cadillac offered ABS on very few models. These very first systems used analog computers and vacuum-

actuated modulators. Since the vacuum-actuated modulators cycled so slowly, the vehicle's actual stopping distance increased. Legal concerns then literally put the development on hold in the US, while the European companies took the lead in the next 10-20 years. In the late 70's, Mercedes and BMW introduced electronically-controlled ABS systems. By 1985, Mercedes, BMW and Audi had introduced Bosch ABS systems and Ford introduced its first Teves system. By the late-80's, ABS systems were offered on many high-priced luxury and sports cars. Today, braking systems on most passenger cars and many light-duty vehicles have become complex, computer-controlled systems. Since the mid-80's, vehicle manufacturers have introduced dozens of anti-lock braking systems. These systems differ in their hardware configurations as well as in their control strategy (SAE, 1992) (Burckhardt, 1993).

For conventional ABS systems, the basic control algorithm is a combination of wheel acceleration/deceleration control and the wheel slip control. The hydraulic brake actuators in these systems have three states:

- Increase
- Hold
- Decrease

The system activates the brake valves when the wheel deceleration is below a specific threshold. Then depending on the slip and the deceleration values of the wheel the states are chosen to achieve a slip value that oscillates around the "critical slip". Hence the friction coefficient between the road and the tire is very close to its maximum. In figure 1.1 a typical control cycle of an ABS system with hydraulic brakes is given.

Conventional ABS systems are very limited in tracking the desired slip value within an acceptable range. Their performance is negatively affected by disturbance. Since their control algorithm depends on the pre-configured threshold values that vary for each braking scenario, it requires a large amount of field testing to achieve the required data. It is also known that these types of

ABS systems have fluctuations (because of their control method) that are noticeable by the driver and have negative effects on the vehicle hardware.
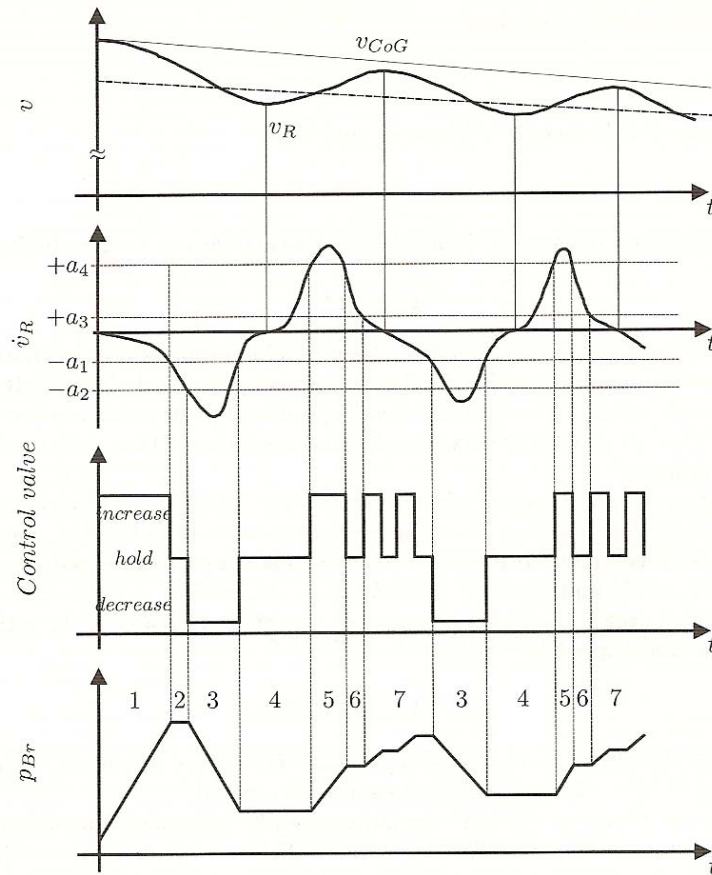
FIGURE 1.1: A TYPICAL CONTROL CYCLE OF AN ABS WITH HYDRAULIC BRAKES.

To overcome the limitations of the conventional systems most of the current ABS systems does not have any hydraulic or mechanical connection between the brake pedal and the actuators. The brake pedal signals are sent to the electronic control unit (ECU) via control area network (CAN). And the hydraulic actuators are replaced with electro-hydraulic or electro-mechanical actuators that allow continuous adjustment of the break force. Figure 1.2 below shows the evolution of the brake systems from the beginning of the 20th century till now.
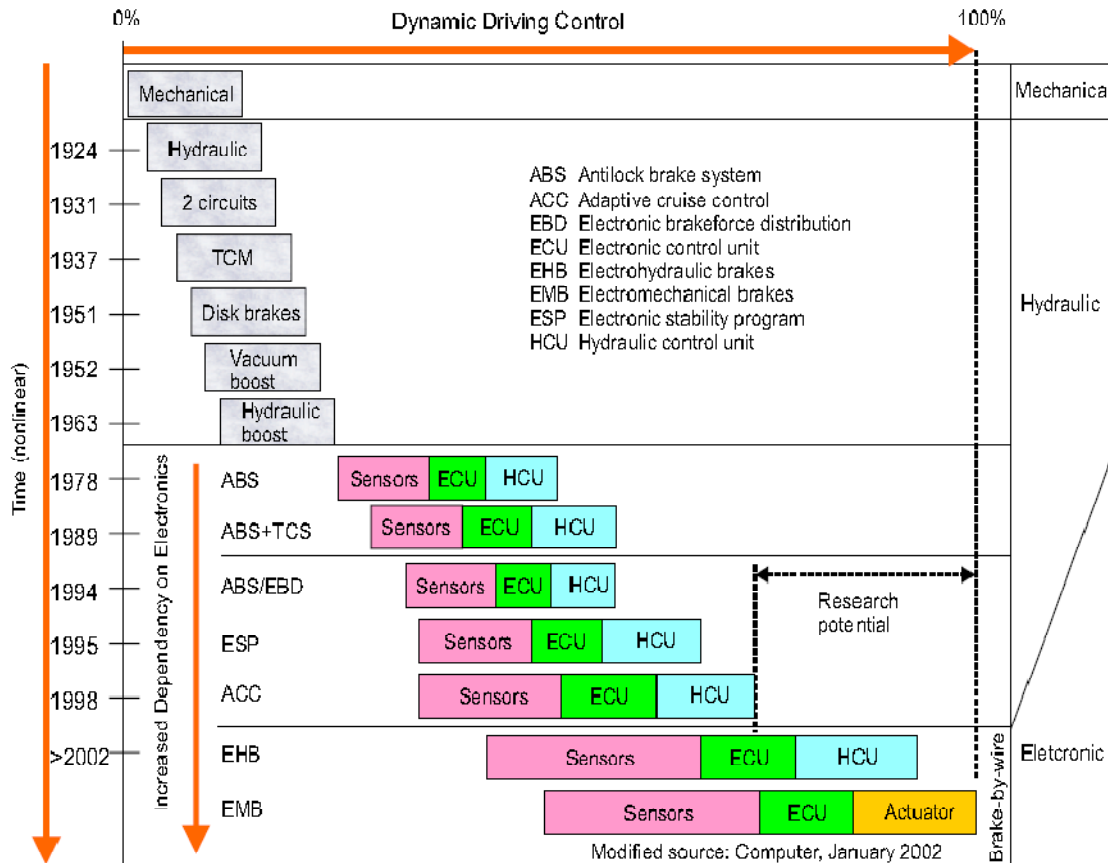
FIGURE 1.2: THE EVOLUTION OF THE BRAKE SYSTEMS.

1.2 Literature Review

Several solutions for ABS based on different control algorithms have been proposed. A sliding mode approach in (Drakunov, Ozguner, Dix, & Asrafi, 1995) applies a search for the optimum brake torque. This approach requires the tire force, hence, a sliding observer is used to estimate it. The approach is tested in a simplifed simulation environment. Another sliding mode approach is proposed in [unsal]. In this approach observability of the system is investigated. An extended kalman filter and a sliding mode observer are compared via simulations. Also in [ozguner, utkin] optimization methods via sliding mode have been proposed.

Another theoretical approach is presented by (Freeman, 1995). Freeman designs an adaptive Lyapunov-based nonlinear wheel slip controller. This controller has been extended in (Yu, 1997) by introducing speed dependence of the Lyapunov function and also including a model of the hydraulic circuit dynamics. Neither of hese two latter approaches have been tested in simulation or in a real vehicle.

A robust PID controller based on loop-shaping and a nonlinear PID, where the nonlinear function gives a low/high gain for large/small errors respectively, are proposed in (Jiang, 2000) together with simulation results for a heavy vehicle. Other PID-type approaches to wheel slip control are considered in (Jun, 1998) (Solyom & Rantzer, 2002).

1.3 Outline

Chapter 2 describes the system model. The wheel dynamics for the quarter car model is given at first. Then the vehicle dynamics and the overall system model including the system equations are explained. Finally, the tire-road friction curves as a function of slip and previously proposed friction models are presented in friction model part.

Chapter 3 explains the proposed controllers. The wheel slip controller to track a desired slip value is presented and then the self optimization method is explained.   Each description the controllers are followed by their simulation results in the Matlab/Simulink environment. The friction force controller for the stabilization of the vehicle is the third part of this chapter. The chapter ends with the description and the simulations of the friction force observer.

Chapter 4 starts with the description of the experimental setup, giving and insight to the IPG's CarMaker program.   Then the experimental results are presented followed by the conclusion.

2 System Model

In this chapter the overall system model and its subsystems are described. We start with the dynamics of the wheel and the vehicle, then continue with the friction model and end with the summary of the system equations. To avoid unnecessary repetition of the equations for each wheel all the subsystems will be explained based on the quarter car model throughout this chapter.

Figure 2.1 shows the overall system structure. Although engine & driveline subsystem is shown in the figure, the engine torque is disabled during braking; hence the only control input is created by the ABS.
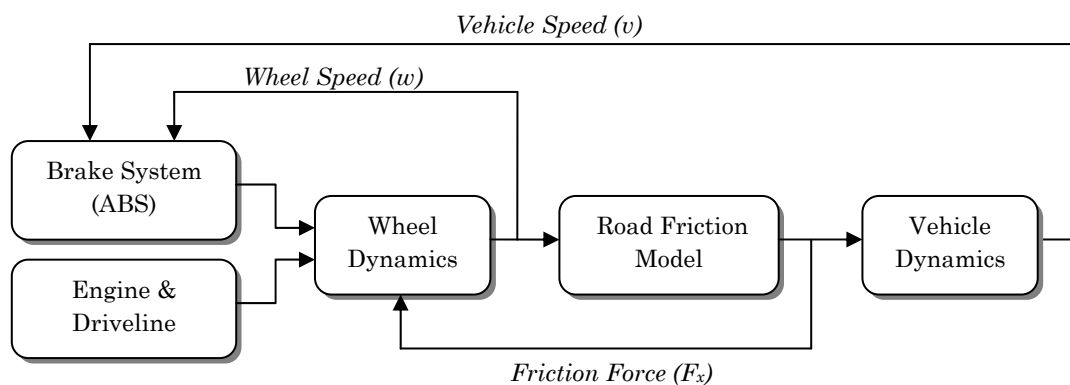
FIGURE 2.1: THE OVERALL SYSTEM STRUCTURE.

2.1 Wheel & Vehicle Dynamics

2.1.1 Wheel Dynamics:

The wheel model is shown in Figure 2.2. As engine torque is applied, the wheel rotates and a tire-road friction force opposing this motion is generated. Then this friction force will accelerate the vehicle along its direction. During braking the wheel already has an angular momentum. Since the engine torque is assumed to be zero the brake torque will result in a negative angular acceleration of the wheel. Hence the direction of the friction force will be reversed, slowing down the

vehicle. Also other forces like wheel viscous friction and wind drag forces should be taken into account all the time.
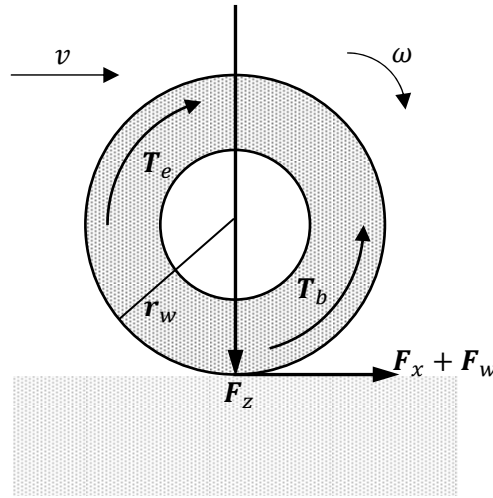
FIGURE 2.2: WHEEL DYNAMICS

The dynamic equation for the angular motion of the wheel is:

$$\dot{\omega}_w = \frac{1}{J_w}[T_e - T_b - r_w(F_x + F_w)] \tag{2.1}$$

where,

ω_w : Angular speed of the wheel

J_w : Moment of inertia of the wheel

T_e : Shaft torque from engine

T_b : Brake torque

r_w : Radius of the wheel

F_x : Tire Friction (Traction) Force

F_z : Vertical force (for quarter vehicle)

F_w : Wheel viscous friction

The tire friction force F_x is given by:

$$F_x = F_z\mu(\lambda, \alpha) \tag{2.2}$$

Where the friction coefficient "μ" is a non-linear function of:

λ_l : Longitudinal tire slip

α : Slip angle of the wheel

7

And longitudinal tire slip is given by:

$$\lambda_l = \frac{\omega_w r_w \cos\alpha - w_x}{w_x} \text{ , while Braking } (\omega_w r_w \cos\alpha \leq w_x) \tag{2.3}$$

$$\lambda_l = \frac{\omega_w r_w \cos\alpha - w_x}{\omega_w r_w \cos\alpha} \text{ , while Accelerating } (\omega_w r_w \cos\alpha \leq w_x)$$

And tire side slip is calculated by:

$$\lambda_s = \frac{\omega_w r_w \sin\alpha}{w_x} \qquad \text{ , while Braking } (\omega_w r_w \cos\alpha \leq w_x) \tag{2.4}$$

$$\lambda_s = \tan\alpha \qquad \text{ , while Accelerating } (\omega_w r_w \cos\alpha \leq w_x)$$

The resultant tire slip is the geometric sum of the side and longitudinal slip values:

$$\lambda_{res} = \sqrt{\lambda_s{}^2 + \lambda_l{}^2} \tag{2.5}$$

where w_x is the longitudinal velocity of the wheel.

If the vehicle drives without the tire side slip, the wheel slip is simply the difference between the rotational equivalent wheel velocity and the center of gravity (CoG) velocity (Kiencke & Nielsen, 2000). Since the slip value should always be smaller than or equal to 1 the speed difference is divided by the respective larger speed, i.e. $\omega_w r_w \cos\alpha$ when accelerating and w_x for Braking. In the rest of thesis we'll assume the slip angle to be zero and for ease of notation we'll refer λ as the longitudinal slip instead of λ_l. The slip value of $\lambda = 0$ characterizes the free motion of the wheel where there is no friction force. And when the wheel is locked, $\lambda = 1$.
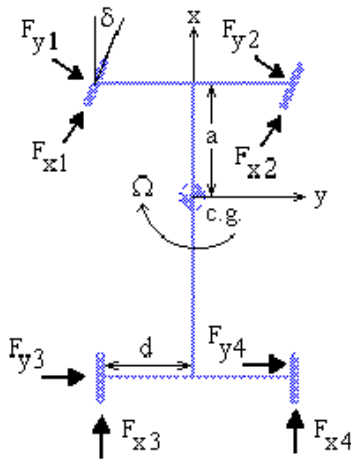
FIGURE 2.3: VEHICLE DYNAMICS

In Figure 2.3 the vehicle dynamics layout is given where the active forces on the x-y plane are shown. The forces $F_{x1}, F_{x2}, F_{x3}, F_{x4}, F_{y1}, F_{y2}, F_{y3}, F_{y4}$ are the longitudinal and the lateral friction forces of the front left, front right, rear left and rear right wheels respectively. Ω is the yaw rate of the vehicle and δ is the steering angle of the wheel (should not be mixed with the side slip angle α in equation 2.3 which is the angle between the velocity vector of the wheel and the wheel axis; Figure 2.4 shows how these values are calculated). The distance from the axle to the center of gravity of the car is a and d is half of the track width.
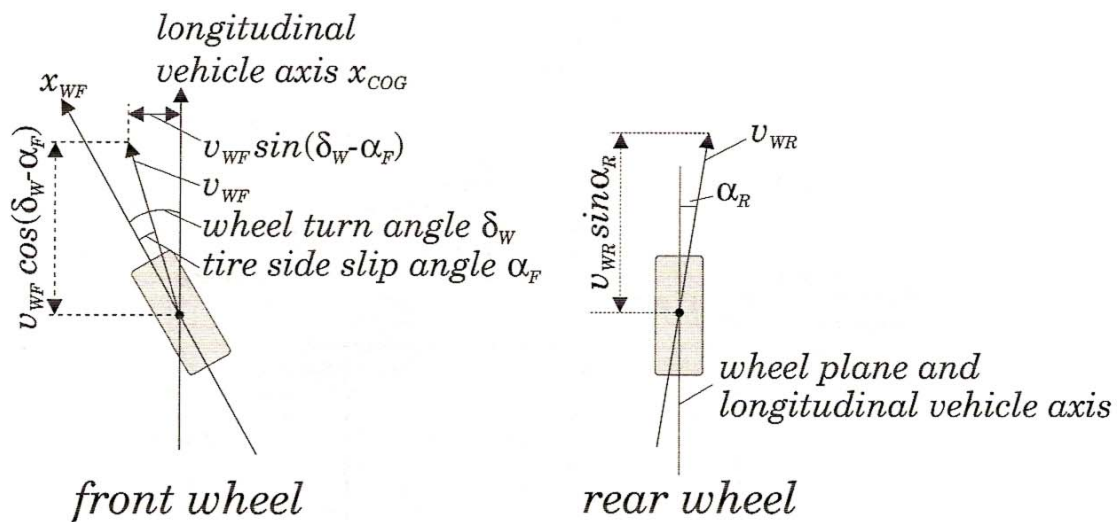
FIGURE 2.4: TIRE SLIP ANGLE AND STEERING ANGLE

The wheel longitudinal velocity of each wheel is given by:

$$w_{x1} = (v_x + \Omega d)cos\delta + (v_y + \Omega a)sin\delta \tag{2.6}$$

$$w_{x2} = (v_x - \Omega d)cos\delta + (v_y + \Omega a)sin\delta \tag{2.7}$$

$$w_{x3} = v_x + \Omega d \tag{2.8}$$

$$w_{x4} = v_x - \Omega d \tag{2.9}$$

Note that, for a straight line maneuver ($\delta = 0$), on a consistent surface ($\Omega = 0$) the wheel longitudinal velocity will be simply $w_x = v_x$. We'll also make the same assumptions in our calculations for simplicity.

2.1.2 Vehicle Dynamics

The dynamic equation for the longitudinal motion of the vehicle is:

$$\dot{v} = \frac{1}{m}(N_w F_x - F_v)$$

$$\tag{2.10}$$

where,

m : Total mass of the vehicle

N_w : Number of wheels

F_v : Aerodynamic drag force ($F_v = \frac{1}{2}\rho C_d A_f v^2$)

The acceleration of the vehicle is equal to the difference between the total friction force available at the tire-road contact point and the aerodynamic drag on the vehicle, divided by the mass of the vehicle.

2.1.3 Combined System and the Slip

Now, we would like to combine the wheel, vehicle and slip dynamics together and create dynamics equations of the overall system. Choosing our states to be:

$$x_1 = \omega_x = \frac{w_x}{r_w} \quad , \quad x_2 = \omega_w \tag{2.11}$$

Differentiating both sides and using the equations (2.1) and (2.10), we get:

$$\dot{x}_1 = -f_1(x_1) + b_{1N}\mu(\lambda) \tag{2.12}$$

$$\dot{x}_2 = -f_2(x_2) + b_{2N}\mu(\lambda) + b_{3N}T \tag{2.13}$$

where,

$$f_1(x_1) = \frac{F_v(x_1)}{mr_w} \qquad b_{1N} = \frac{F_z N_w}{mr_w} \qquad b_{3N} = \frac{1}{J_w}$$

$$f_2(x_2) = \frac{F_w(x_2)}{J_w} \qquad b_{2N} = \frac{r_w F_z}{J_w} \qquad T = -T_b\lambda$$

Using equations (2.3) and (2.11) we can easily calculate the slip in terms of the states:

$$\lambda = \frac{x_2 - x_1}{x_1} \tag{2.14}$$

Taking the time derivative of the both sides:

$$\dot{\lambda} = \frac{\dot{x}_2 - (1 + \lambda) \cdot \dot{x}_1}{x_1} \tag{2.15}$$

Substituting equations (2.12) and (2.13) into (2.15) we can get the state space equations of the system:

$$\dot{\lambda} = f + b \cdot u \tag{2.16}$$

$$f = \frac{[(1 + \lambda) \cdot f_1(x_1) - f_2(x_2)] - [b_{2N} + (1 + \lambda) \cdot b_{1N}] \cdot \mu(\lambda)}{x_1}$$

$$u = \frac{T}{x_1}, b = b_{3N}.$$

The equations above will be used in the 3rd chapter where we'll define our control algorithm to reach a desired slip value.

2.2 Friction Model

The friction force plays a major role in both wheel and vehicle dynamics so it should be modeled and understood well. Rewriting equations (2.2) and (2.3):

$$F_x = F_z \mu(\lambda, \alpha)$$

$$\lambda = \frac{\omega_w r_w cos\alpha - w_x}{w_x}$$

By looking at the equations we can see that the friction force has a nonlinear relationship with the slip, hence with the wheel and the vehicle velocities. Also although we'll assume F_z (the normal force at the tire-road contact point) to be static, because of the dynamics of the suspension system it actually introduces additional nonlinearity to the system in the real case.

2.2.1 Friction Coefficient Calculation

The nonlinearity between the friction coefficient and the tire slip is shown in the Figure 2.5.
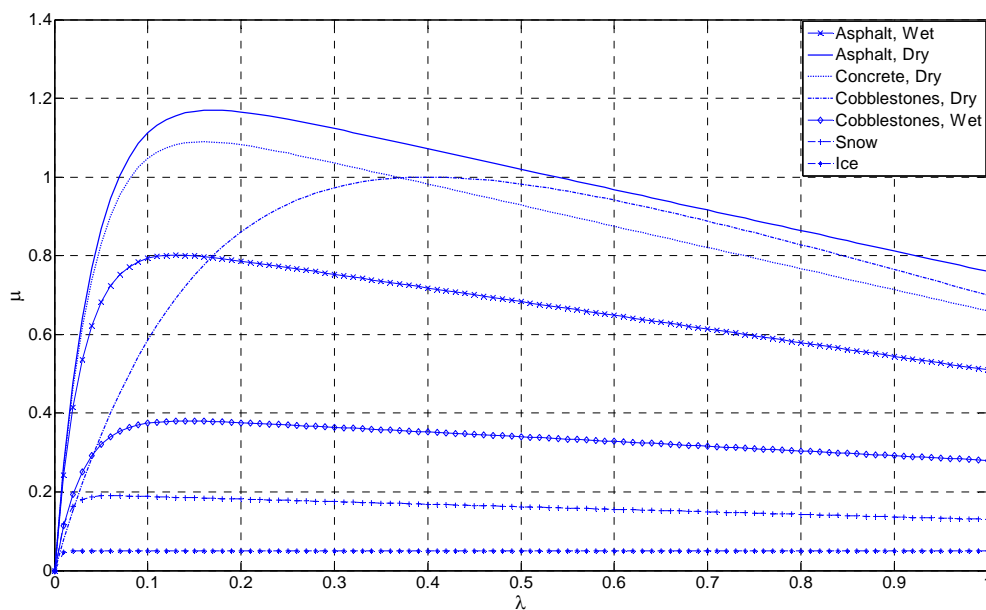

FIGURE 2.5: FRICTION COEFFICIENT (μ) – TIRE LONGITUDINAL SLIP (λ) CURVE

The major characteristic of the friction coefficient is that as the slip increases from *0* to *1* it reaches a maximum value, which we'll call it μ_p and the corresponding slip value λ_p, and then it starts decreasing till it reaches its minimum where the wheel is locked and only sliding friction force will act on the wheel. The friction coefficient has the same sign with the slip value, meaning that during braking both the slip and the friction coefficient is negative.

Several tire friction models have been proposed to describe the nonlinear behavior of the friction coefficient. On 1987 Bakker, Nyborg and Pacejka proposed one of the most reputed tire models also known as the "magic formula" which suitably fits the experimental data. It is of the form:

$$\mu(\lambda_x) = D sin(C \arctan(B\lambda_x - E(B\lambda_x - \arctan(B\lambda_x))))$$

where *B-E* characterizes the model.

The model in (Burckhardt, 1993) is derived in a similar manner and given as:

$$\mu(\lambda_x) = C_1\left(1 - e^{-C_2 2*\lambda}\right) - C_3\lambda \tag{2.17}$$

where the parameters are defined as:

C_1: maximum value of the friction curve

C_2: shape characteristic of the friction curve

C_3: the difference between the maximum value and the value at $\lambda = 1$

This model is also extended in (Kiencke & Nielsen, 2000) which is:

$$\mu(\lambda_x) = \left(C_1\left(1 - e^{-C_2\lambda}\right) - C_3\lambda\right)e^{-C_4\lambda v}(1 - C_4 F_z^2)$$

where the additional parameters are define as:

C_4: the influence of the higher drive velocity

C_5: the influence of the higher wheel load

Both factors have a maximum value of 1; hence they lead to a reduction of the friction coefficient. Incorrect tire pressure can also lead to a reduction of the friction coefficient (Kiencke & Nielsen, 2000)

In Figure 2.6 (Kiencke & Nielsen, 2000) parameters for various road conditions are shown. The friction coefficients in figure 2.5 are calculated using equation 2.17 with these values.

Surface	c_1	c_2	c_3
Asphalt, dry	1.2801	23.99	0.52
Asphalt, wet	0.857	33.822	0.347
Concrete, dry	1.1973	25.168	0.5373
Cobblestones, dry	1.3713	6.4565	0.6691
Cobblestones, wet	0.4004	33.7080	0.1204
Snow	0.1946	94.129	0.0646
Ice	0.05	306.39	0

FIGURE 2.6: PARAMETER SETS FOR EQUATION 2.17 ON VARIOUS SURFACES.

In the simulations we used the friction coefficient model from (Unsal & Kachroo, 1999), which is:

$$\mu(\lambda_x) = \frac{2\mu_p \lambda_p \lambda}{\lambda_p^2 + \lambda^2}$$

where μ_p and λ_p are the peak values of the friction coefficient and the slip respectively.

2.2.2 Characteristics of the Friction Coefficient

It is seen from Figure 2.5 that the curve characteristics vary according to the surface conditions. The value of the friction coefficient is smaller in wet and icy conditions. In Figure 2.7 the maximum friction coefficient values are given.

Surface	μ_p
Asphalt, Dry	1.1~1.2
Concrete, Dry	1.0~1.1
Cobblestones, Dry	1.0
Asphalt, Wet	0.5~0.6
Concrete, Wet	0.8
Cobblestones, Wet	0.3~0.4
Gravel	0.6
Snow	0.2
Ice	0.1

FIGURE 2.7: MAXIMUM μ_p VALUES ON VARIOUS SURFACES.

Also we can see from the equation 2.3 that the longitudinal slip has a sinusoidal relationship with the tire slip angle. Figure 2.8 (Kiencke & Nielsen, 2000) shows the longitudinal friction coefficient over the longitudinal slip with respect to different tire slip angles. As the tire slip angle increases the longitudinal force decreases. If the driver turns or a yaw moment occurs because of the difference in the brake force distribution on the wheels the result is a tire side slip angle together with a side force. This causes a reduction in the longitudinal force and the braking distance is increased. For stable driving no slip angle greater than $\alpha = 16°$ can occur, as the vehicle body side slip angle lies in a similar value range (Kiencke & Nielsen, 2000). As it is seen in the figure for $\alpha = 16°$ we have almost 15% loss in the longitudinal force. Also one more important issue we can get by looking at Figure 2.8 is that the position of the extremum point of the friction coefficient is shifted to a larger value of longitudinal slip. We'll see the importance of this point in the 3rd chapter.
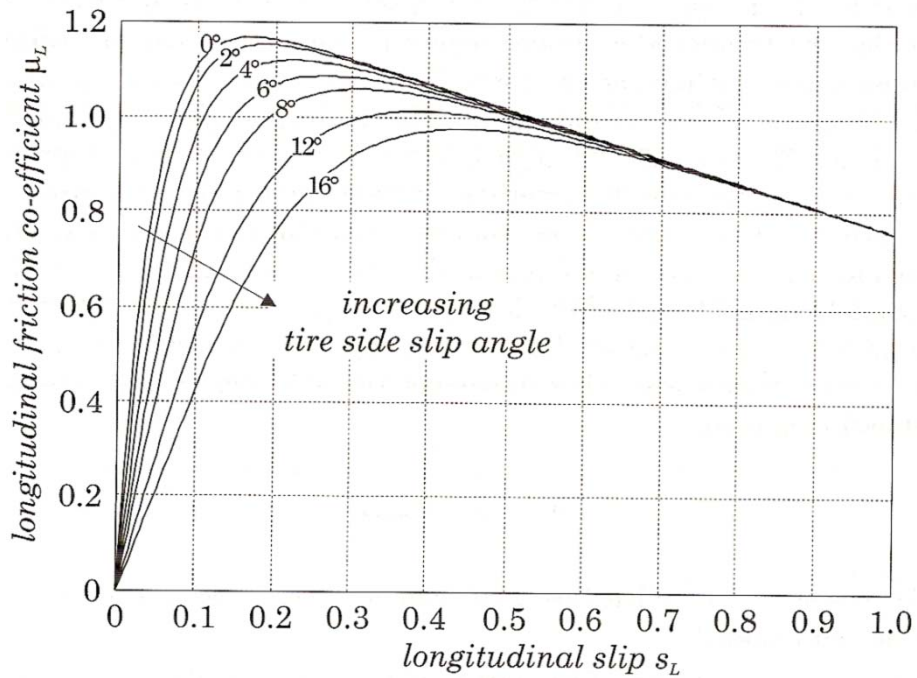
FIGURE 2.8: LONGITUDINAL FRICTION COEFFICIENT OVER LONGITUDINAL SLIP.

Figure 2.9 (Kiencke & Nielsen, 2000) shows the lateral friction coefficient versus longitudinal friction coefficient for different tire slip angles. It is obvious that as the angle increases the longitudinal force decreases. Again for $\alpha = 16°$ the longitudinal friction coefficient can be almost 1.0. Another important thing to be considered is that although the friction coefficient remains 0 all the time for $\alpha = 0°$, for $\alpha = 2°$ the lateral friction coefficient can reach a value of 0.7 which is considerably large. This is one of the main motivations of the development of the stability control systems, to keep the vehicle motion and wheel motion as aligned as possible.
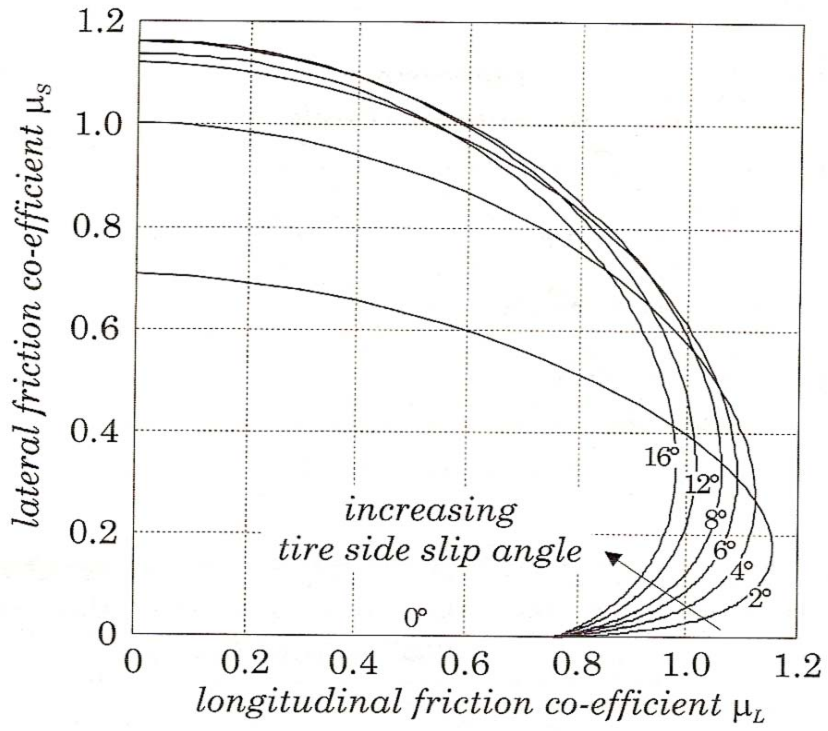
FIGURE 2.9: LATERAL FRICTION COEFFICIENT AGAINST LONGITUDINAL FRICTION COEFFICIENT.

3 Sliding Mode Control of ABS

3.1 Introduction

The term "sliding mode control" first appeared in the context of variable-structure systems. Soon sliding modes became the principal operational mode for this class of control systems. Practically all design methods for variable-structure systems are based on deliberate introduction of sliding modes which have played, and are still playing, exceptional role both in theoretical developments and in practical applications. Due to its order reduction property and its low sensitivity to disturbances and plant parameter variations, sliding mode control is an efficient tool to control complex high-order dynamic plants operating under uncertainty conditions which are common for many processes of technology. (Utkin, Sliding Mode Control in Electromechanical Systems, 1999)

In late fifties in the Soviet Union, to solve control problems of second order systems initially variable structure control (VSC) appeared. The idea of the pioneers of the field was to switch among two or more controls to obtain improved, mathematically stable control system performance. Switching among control inputs to the plant leads to a system defined with a differential equation with a discontinuous right-hand side, hence the name "Variable Structure System (VSS)". Sliding mode control (SMC) is a particular type of Variable structure system control. Sliding modes may appear in a dynamic system governed by ordinary differential equations with discontinuous right-hand sides. SMC is characterized by a discontinuous control action, which changes structure upon reaching a set of predetermined switching surfaces. This kind of control may result in a very robust system and thus provides a possibility for achieving the goals of high-precision and fast response. The main advantages of this type of control are:

- The order of the motion can be reduced.

- The motion equation of the sliding mode can be designed linear and homogenous, despite that the original system may be governed by nonlinear equations.
- The sliding mode does not depend on the process dynamics, but is determined by parameters selected by the designer.
- Once the sliding motion occurs, the system has invariant properties which make the motion independent of certain system parameter variations and disturbances. Thus the system performance can be completely determined by the dynamics of the sliding manifold.

After each controller design, corresponding results of the Matlab/Simulink simulations are given. The system parameters used for the simulation are selected as follows:

$J_w = 13.75 kgm^2$, $R_w = 0.326m$, $M_{car} = 1500kg$, $M_{wheel} = 40kg$, $f_0 = 0.01, f_s = 0.005,$

$A_f = 2.04m^2, C_d = 0.539$.

The max applicable brake torque is limited to 1500Nm. λ_p, μ_p values may vary according to different scenarios.

3.2 Wheel Slip Control

3.2.1 Sliding Mode Control of the Wheel Slip

Our motivation for using SMC in ABS control arises from the capabilities of the sliding mode control stated above. ABS system has nonlinearities, due to the rapid changes and high disturbance in the system our control should be highly robust to uncertainties and disturbance and also should be fast enough to handle the nonlinearities. Rewriting the equation 2.16:

$$\dot{\lambda} = f + b \cdot u \tag{3.1}$$

$$f = \frac{[(1 + \lambda) \cdot f_1(x_1) - f_2(x_2)] - [b_{2N} + (1 + \lambda) \cdot b_{1N}] \cdot \mu(\lambda)}{x_1}$$

$$u = \frac{T}{x_1}, b = b_{3N}$$

Where

$$f_1(x_1) = \frac{F_v(x_1)}{mr_w} \qquad\qquad b_{1N} = \frac{F_z N_w}{mr_w} \qquad\qquad x_1 = \omega_x = \frac{w_x}{r_w}$$

$$f_2(x_2) = \frac{F_w(x_2)}{J_w} \qquad\qquad b_{2N} = \frac{r_w F_z}{J_w} \qquad\qquad x_2 = \omega_w$$

$$T = -T_b \lambda \qquad\qquad b_{3N} = \frac{1}{J_w}$$

If we look at the equation (3.1) we can see that it is nonlinear and involves uncertainties in its parameters. The nonlinear characteristic of the equation is caused by the following factors (Unsal & Kachroo, 1999):

- The relationship of wheel slip with wheel velocity and vehicle velocity is nonlinear.
- The $\mu - \lambda$ relationship is nonlinear.
- There are multiplicative terms in the equation.
- The functions $f_1(x_1)$ and $f_2(x_2)$ are nonlinear.

The main idea in applying SMC is to handle these nonlinearities and uncertainties in the system.

Our aim is to track a reference wheel slip. Hence the control objective is to drive the system states $(\lambda, \dot{\lambda})$ to the desired values $(\lambda_d, \dot{\lambda}_d)$. Defining the switching surface s to be:

$$s = \lambda - \lambda_d \tag{3.2}$$

The sliding motion will occur when the states $(\lambda, \dot{\lambda})$ reach the sliding surface $s=0$. We'll apply the *equivalent control method* where we'll define our *hitting control input* which will force the states to sit on the sliding surface and *equivalent control input* which is the input that will move the states along the sliding surface. The sum of these two inputs will give us our *total control input*. Since for the ABS system the control input is the brake torque from now on we'll call the equivalent, hitting and total control inputs as equivalent torque T_{eq}, hitting torque T_h and total torque T respectively.

Let's first find the equivalent torque. Assuming that we are on the sliding surface we have:

$$s = 0 \, , \ \dot{s} = 0 \tag{3.3}$$

Differentiating equation 3.2 and substituting into equation 3.3, we get:

$$\dot{\lambda} = \dot{\lambda}_d \tag{3.4}$$

Substituting equation 3.1 into 3.5, we get our equivalent input:

$$u_{eq} = -b^{-1}(f - \dot{\lambda}_d) \tag{3.5}$$

Since there are uncertainties in f such because of the friction coefficient $\mu(\lambda)$ and the normal force F_z , f is replace by its estimate. Resulting in the estimated equivalent input:

$$\hat{u}_{eq} = -b^{-1}(\hat{f} - \dot{\lambda}_d) \tag{3.6}$$

It is assumed that the estimation error of the f is bounded by some positive value F such that $|f - \hat{f}| \leq F$. Now we should find our hitting torque. Choosing our hitting control input to be:

$$u_h = -b^{-1}(ksign(s)) \, , \ where \ k \geq 0 \tag{3.7}$$

Our total estimated input becomes:

$$\hat{u}_t = \hat{u}_{eq} + u_h$$
$$\hat{u}_t = -b^{-1}(\hat{f} + ksign(s) - \dot{\lambda}_d) \tag{3.8}$$

For finding the stability criteria for this system, we choose our Lyapunov function to be:

$$\frac{1}{2}s^T s > 0 \tag{3.9}$$

Taking the derivative and forcing it to be smaller than or equal to 0, equation 3.9 becomes:

$$s\dot{s} \leq 0 \tag{3.10}$$

Substituting   equation 3.8 into 3.1, we get:

$$\underbrace{\dot{\lambda} - \dot{\lambda}_d}_{\dot{s}} = |f - \hat{f}| - ksign(s) \tag{3.11}$$

Substituting 3.11 into 3.10:

$$s|f - \hat{f}| - k \underbrace{ssign(s)}_{|s|} \leq 0$$

Since $|f - \hat{f}| \leq F$, if k is chosen such that $k > F$, the exponential convergence of the system is guaranteed.

Then our equivalent, hitting and total control torque values are:

$$\hat{T}_t = \hat{u}_t x_1 \tag{3.12}$$

$$\hat{T}_t = \underbrace{-b^{-1}(\hat{f} - \dot{\lambda}_d)x_1}_{\hat{T}_{eq}} - \underbrace{b^{-1}ksign(s)x_1}_{T_h}$$

Although the control guaranties exponential convergence there is one important point that should be considered. If we look at the equation 3.1, we can see that as $v \to 0$ the open loop slip dynamics from T_t to λ become infinitely fast with infinite high-frequency gain. To avoid this slip controller should be switched off for small v.

Also another problem in sliding mode control arises from the high frequency switching of the control input, called *chattering*. This can be avoided by replacing the signum function with the saturation function.

3.2.2 Simulation Results for Slip Control

In the simulation, at first the desired slip value is set to $\lambda_d = -0.12$ value and than a sinusiodal input is applied to see the tracking performance. The actual slip, the error function, the applied brake torque and the wheel& vehicle velocities are shown.

Results for $(\lambda_d = -0.12)$:
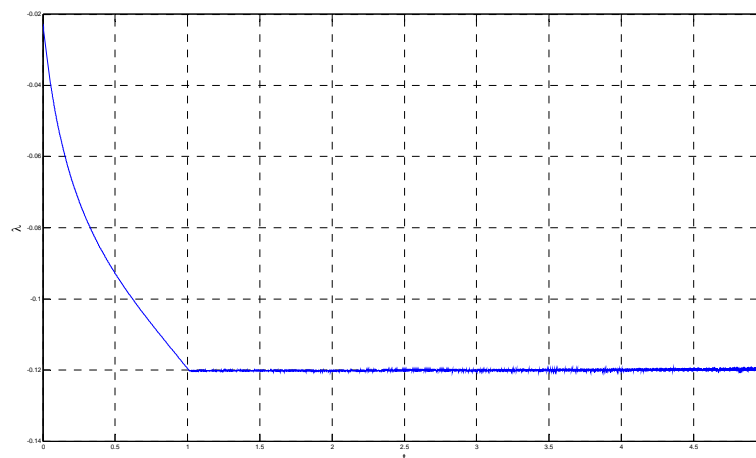
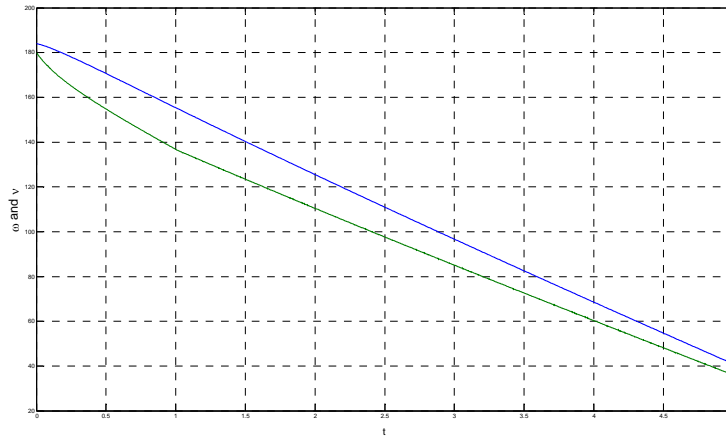FIGURE 3.1: SLIP VS TIME (SMC SLIP CONTROLLER)

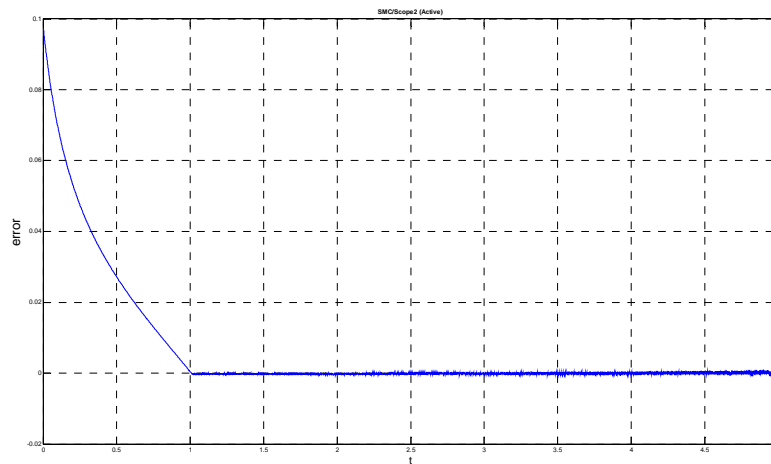FIGURE 3.2: WHEEL AND VEHICLE VELOCITIES (SMC SLIP CONTROLLER)

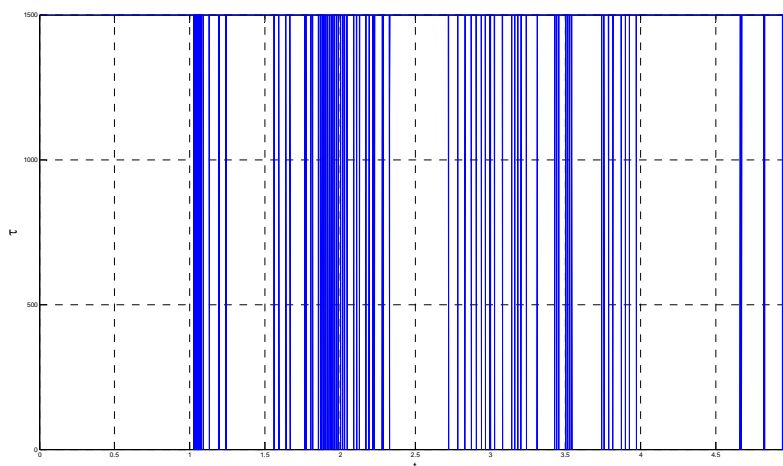FIGURE 3.3: CONTROLLER ERROR (SMC SLIP CONTROLLER)

FIGURE 3.4: BRAKE TORQUE (SMC SLIP CONTROLLER)

As we can see from the figures the controller reaches the desired slip in a second continues to stay on the sliding surface. The wheel is not locked.

Results for the tracking ($\lambda_d = -0.1 + 0.05 \sin(2\pi ft)$ _where_ $f = \pi/2$):
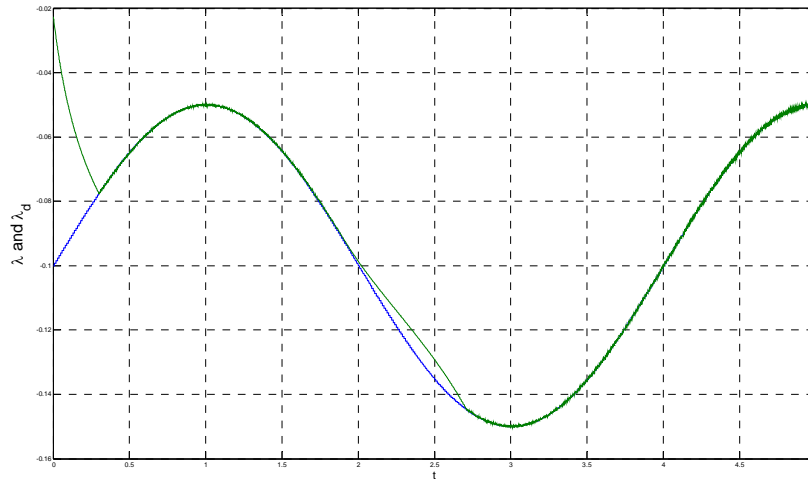

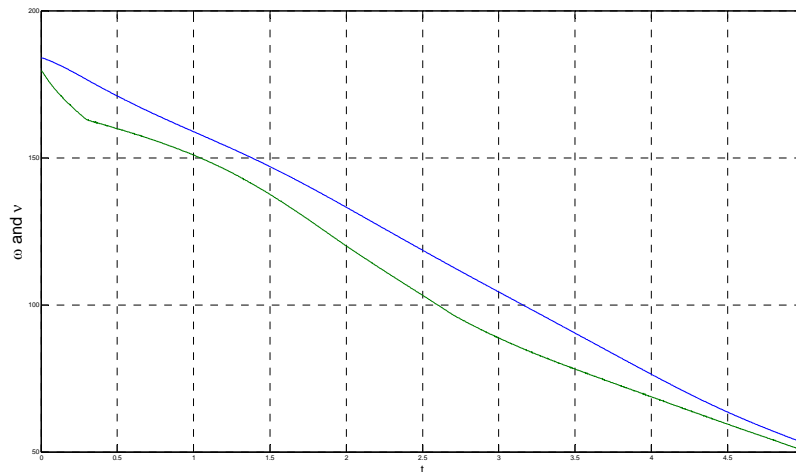FIGURE 3.5: λ VS λ_d (SMC SLIP CONTROLLER- TRACKING)

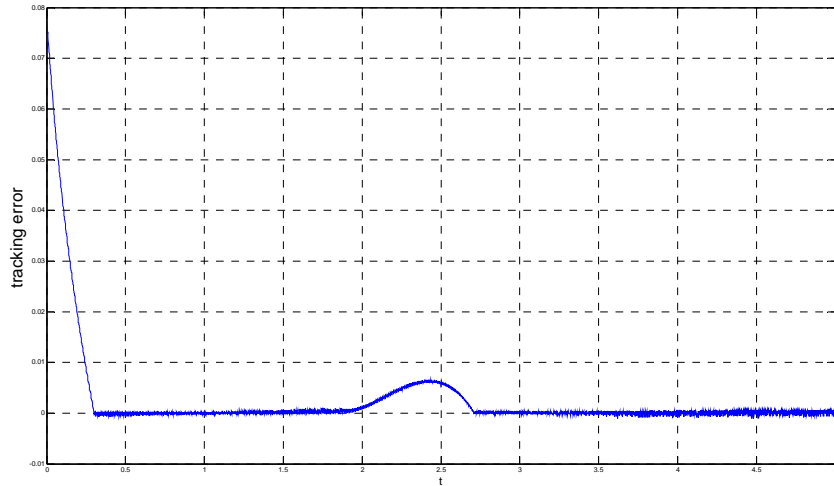FIGURE 3.6: WHEEL AND VEHICLE VELOCITIES (SMC SLIP CONTROLLER- TRACKING)

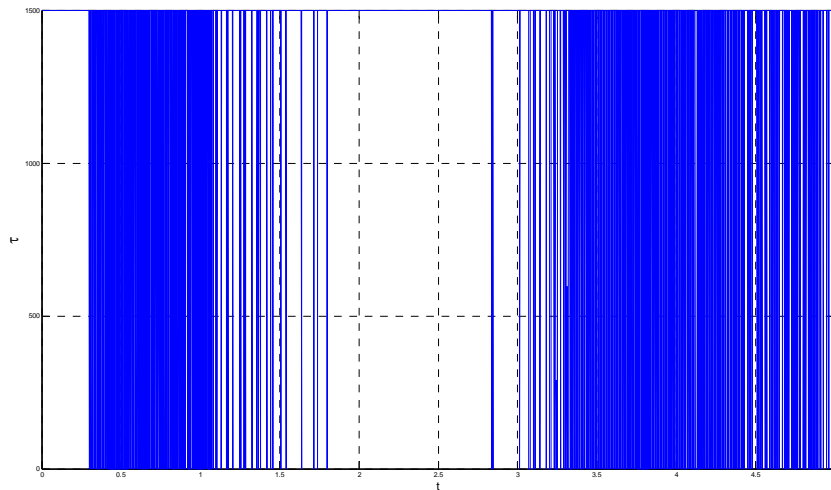FIGURE 3.7: TRACKING ERROR (SMC SLIP CONTROLLER- TRACKING)

FIGURE 3.8: BRAKE TORQUE (SMC SLIP CONTROLLER- TRACKING)

We can see from the figures the tracking performance of the controller is satisfactory. The main difference here is when the desired slip decreases although full brake torque is applied the friction torque reduces the effect of the brake torque. Hence this lag in the response of the wheel dynamics results in a small error in tracking. The same simulation result with a brake torque limit of 2000N is given below. The tracking performance is better as we can see.
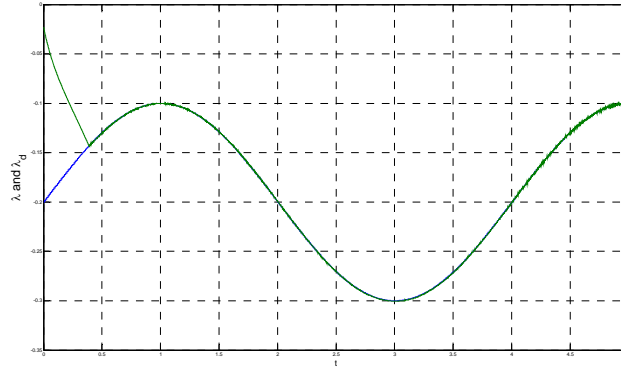
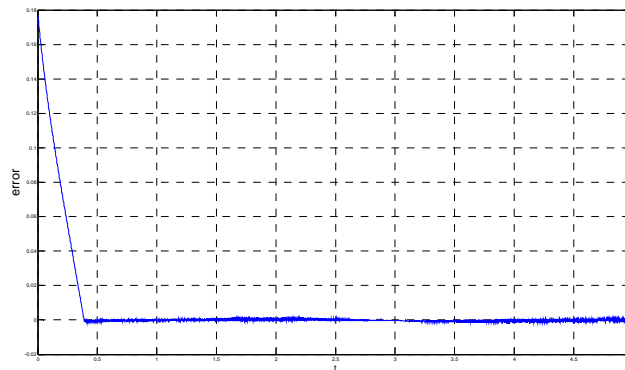FIGURE 3.9: λ VS λ_d (SMC SLIP CONTROLLER- TRACKING, T$_{\text{MAX}}$=2000N)

FIGURE 3.10: TRACKING ERROR (SMC SLIP CONTROLLER- TRACKING, T$_{\text{MAX}}$=2000N)

A similar result occurs also when there is a sharp increase in the desired slip value. Since the engine torque is disabled the wheel dynamics depend entirely on the friction force which limits the response time. An interesting topic arises from this result. If only the vehicle has separate motors driving each wheel the motors can also be triggered to apply positive torque to improve the performance of the ABS. Figures 3.11 and 3.12 shows the system response to a step in λ_d with and without engine torque respectively.

27

FIGURE 3.11: λ VS λ_d (SMC SLIP CONTROLLER- TRACKING, W/O T$_E$)

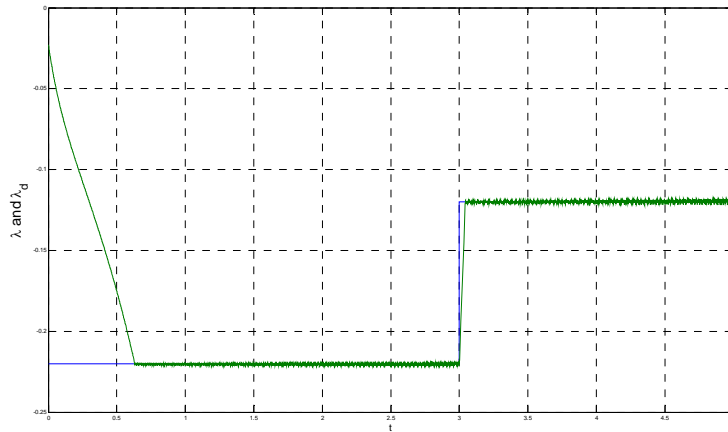
FIGURE 3.12: λ VS λ_d (SMC SLIP CONTROLLER- TRACKING, WITH T$_E$)

3.3 Friction Coefficient Optimization

In part 2.2 we saw that the peak value of the friction coefficient and its corresponding slip value vary depending on the road conditions and tire slip angle. This creates a major problem for the ABS controllers. In most of the systems the desired slip values for different braking scenarios are configured and the controller tracks the preconfigured desired slip value. Because of the

uncertainties and variations in the road and driving conditions it is not possible to find the maximum friction coefficient in most of the cases.

In the previous part we designed a controller for tracking a desired slip value. However, only the slip controller itself does not guarantee the maximum friction force. We have to implement a self-optimization controller that will always force the friction coefficient sit on the top of the friction coefficient-wheel slip curve. There are some friction force optimization techniques proposed for the ABS system in the literature (Utkin, Sliding Modes in Control and Optimization, 1992) (Drakunov, Ozguner, Dix, & Asrafi, 1995). The one we implemented in this project is proposed in (Utkin, Sliding Modes in Control and Optimization, 1992).

3.3.1 Self Optimization via SMC

Since during Braking both the friction coefficient and the slip have negative signs our problem becomes actually a *minimization* problem.

Given a function which has a global minimum:

$$y = f(x) \quad and\ its\ derivative\ is \quad \dot{y} = \frac{\partial f}{\partial x} \dot{x} \tag{3.13}$$

We want to drive *the function y* to its minimum by applying our control input. To achieve this objective, we choose a reference function g and define our control input u and error ε such that:

$$\dot{x} = u \tag{3.14}$$

$$u = u_0\ sign(s_1, s_2) \tag{3.15}$$

$$\varepsilon = g - y \tag{3.16}$$

$$\dot{g} = -\rho + Mv\ (s_1, s_2) \tag{3.17}$$

where,

$g(t)$ is the reference function and u_0, M, ρ are positive constants.

$s_1 \ and \ s_2$ are our sliding surfaces which are defined to be:

$$s_1 = \varepsilon, \qquad s_2 = \varepsilon + \delta \qquad\qquad\qquad (3.18)$$

where,

δ is a positive constant.

The v function is a 3-point relay element whose graph is given in Figure 3.13 below. The hysteresis regions are added to reduce the switching frequency of the controller. The graph of the u function is also given Figure 3.15.
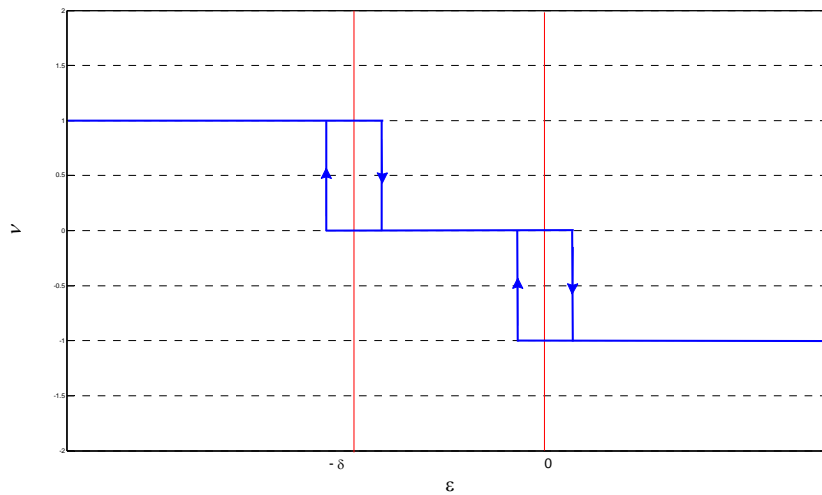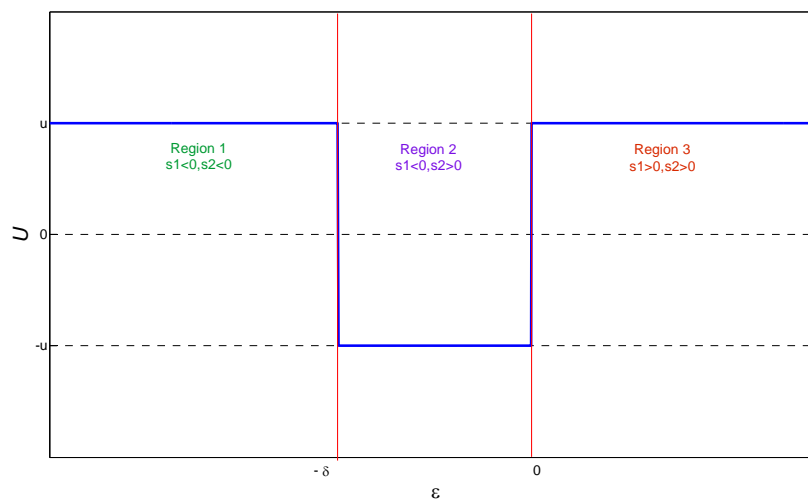

FIGURE 3.13: $v\left(\varepsilon\right)$ FUNCTION

FIGURE 3.14: $u\left(\varepsilon\right)$ FUNCTION

30

If we look at the Figure 3.15 where the flow chart of the controller is shown we can more easily see the idea behind this setup. The controller at first drives the error to a region bounded by delta (region 2). When this region is once reached it modifies the reference function and starts to minimize it (since $\dot{g} = -\rho$, $\rho < 0$ $\forall t$). During his minimization steps control input allows the controller to keep the output of the plant within the error region. When the global minimum is reached the controller starts oscillating and moving in the neighborhood of the global minimum.
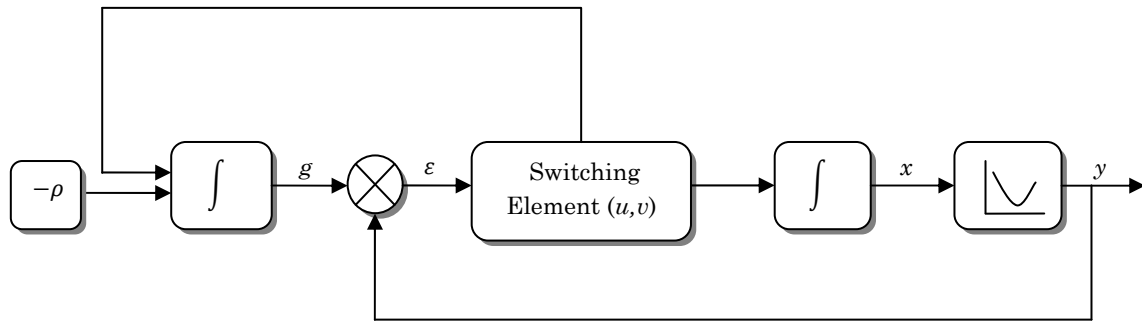

FIGURE 3.15: SELF-OPTIMIZATION CONTROLLER.

For investigating the error dynamics of the controller taking the derivative of the equation 3.15:

$$\dot{\varepsilon} = \dot{g} - \dot{y} \tag{3.19}$$

Substituting equations 3.13, 3.14, 3.15 and 3.17 into equation 3.19, we get:

$$\dot{\varepsilon} = -\rho + M\, v(s_1 s_2) - \frac{\partial f}{\partial x} \underbrace{u_0 sign(s_1 s_2)}_{\dot{x}} \tag{3.20}$$

where,

$$\dot{\varepsilon} = \dot{s}_1 = \dot{s}_2 \tag{3.21}$$

By looking at the equation 3.21 we can say that any of the sliding surfaces will take our error dynamics to 0 and our error to:

$$\varepsilon = 0 \ for \ s_1 = 0 \quad or \quad \varepsilon = -\delta \ for \ s_2 = 0$$

From the figures 3.14 and 3.15 we can say that we have three different regions to investigate the convergence of the controller. The regions are:

- *Region I* : $s_1 < 0$ and $s_2 < 0$
- *Region II* : $s_1 < 0$ and $s_2 > 0$
- *Region III*: $s_1 > 0$ and $s_2 > 0$

For finding the stability criteria for the convergence of the system, we choose our Lyapunov candidate to be:

$$\frac{1}{2}\varepsilon^T \varepsilon > 0 \tag{3.22}$$

Taking the derivative and forcing it to be smaller than or equal to 0, equation 3.9 becomes:

$$\varepsilon \dot{\varepsilon} \leq 0 \tag{3.23}$$

Region I ($s_1 < 0$ and $s_2 < 0$, $\varepsilon < -\delta$):

In this region both switching functions are negative, which leads to:

$$u = u_0 \ and \ v = 1$$

Substituting these values into the error dynamics, equation 3.20 become:

$$\dot{\varepsilon} = -\rho + M - \frac{\partial f}{\partial x}u_0 \tag{3.24}$$

Substituting equation 3.24 into equation 3.23, we get:

$$\varepsilon(-\rho + M - \frac{\partial f}{\partial x}u_0) \ \leq 0$$

Since $(\varepsilon < -\delta)$ our convergence criterion for this region is:

$$-\rho + M - \frac{\partial f}{\partial x}u_0 > 0 \quad \xrightarrow{yields} \quad M > \rho + \left|\frac{\partial f}{\partial x}\right|u_0 \tag{3.25}$$

This will lead to $s_1 \to 0$ and $s_2 \to 0$.

Region II ($s_1 < 0$ and $s_2 > 0$, $-\delta < \varepsilon < 0$):

In this region we have:

$u = -u_0$ $and\ v = 0$

Substituting these values into the error dynamics, equation 3.20 become:

$$\dot{\varepsilon} = -\rho + \frac{\partial f}{\partial x} u_0 \tag{3.26}$$

Substituting equation 3.26 into equation 3.23, we get:

$$\varepsilon(-\rho + \frac{\partial f}{\partial x} u_0) \ \leq 0$$

Since $(-\delta < \varepsilon < 0)$ our convergence criterion for this region is:

$$-\rho + \frac{\partial f}{\partial x} u_0 > 0 \quad \xrightarrow{yields} \quad \left|\frac{\partial f}{\partial x}\right| u_0 > \rho \tag{3.27}$$

Depending on the sign of $\frac{\partial f}{\partial x}$ the system will converge via $s_1\ or\ s_2$:

If $sign\left(\frac{\partial f}{\partial x}\right) > 0$, $s_1 \to 0\ and\ \varepsilon \to 0$ and if $sign\left(\frac{\partial f}{\partial x}\right) < 0$, $s_2 \to 0\ and\ \varepsilon \to -\ \delta$.

Region III ($s_1 > 0$ and $s_2 > 0$, $\varepsilon > 0$):

In this region both switching functions are positive, which leads to:

$u = u_0$ $and\ v = -1$

Substituting these values into the error dynamics, equation 3.19 become:

$$\dot{\varepsilon} = -\rho - M - \frac{\partial f}{\partial x} u_0 \tag{3.28}$$

Substituting equation 3.28 into equation 3.23, we get:

$$\varepsilon(-\rho - M - \frac{\partial f}{\partial x} u_0) \ \leq 0$$

Since ($\varepsilon > 0$) our convergence criterion for this region is:

$$-\rho - M - \frac{\partial f}{\partial x}u_0 < 0 \quad \xrightarrow{yields} \quad M > \left|\frac{\partial f}{\partial x}\right|u_0 \tag{3.29}$$

This will lead to $s_1 \to 0$ and $s_2 \to 0$.

Summing up all the results in all the regions, for exponential convergence of the system the following two constraints must be fulfilled $\forall x$:

- $M > \rho + \left|\frac{\partial f}{\partial x}\right|u_0$
- $\left|\frac{\partial f}{\partial x}\right|u_0 > \rho$

Figure 3.16 below is a summary of what we did above. It shows the criteria and the convergence of the control in all the regions. Since the hysteresis in the transition regions of the v function is to avoid very high frequency switching, for simplicity we neglect those in the figure.

In the ABS scenario, since the function we would like to minimize is the friction coefficient which is a nonlinear function of the wheel slip replacing y with $\mu(\lambda)$ and x with λ will be the only change in the controller.
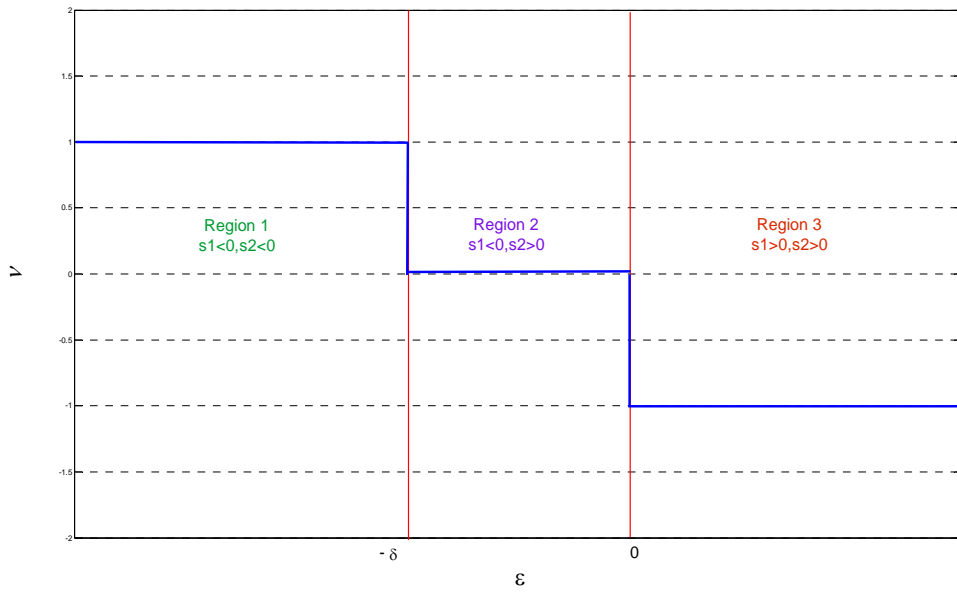
Region I	Region II	Region III
$s_1 < 0 \;\; and \;\; s_2 < 0$	$s_1 < 0 \;\; and \;\; s_2 > 0$	$s_1 > 0 \;\; and \;\; s_2 > 0$
$u = u_0 \; , v = -1$	$u = -u_0 \; , v = 0$	$u = u_0 \; , v = -1$
$\dot{s_1}, \dot{s_2} = -\rho + M - \dfrac{\partial f}{\partial x} u_0$	$\dot{s_1}, \dot{s_2} = -\rho + \dfrac{\partial f}{\partial x} u_0$	$\dot{s_1}, \dot{s_2} = -\rho - M - \dfrac{\partial f}{\partial x} u_0$
Constraint:	*Constraint:*	*Constraint:*
$M > \left\| \dfrac{\partial f}{\partial x} \right\| u_0 + \rho$	$\left\| \dfrac{\partial f}{\partial x} \right\| u_0 > \rho$	$M > \left\| \dfrac{\partial f}{\partial x} \right\| u_0$
$s_1 \to 0 \;\; and \;\;\; s_2 \to 0$	$s_1 \; or \; s_2 \to 0$	$s_1 \to 0 \;\; and \;\;\; s_2 \to 0$
	Depending on $sign(\dfrac{\partial f}{\partial x})$	

FIGURE 3.16: ERROR DYNAMICS OF THE OPTIMIZATION CONTROLLER

3.3.2 Simulation Results for the Optimization Controller

For the simulation of the friction coefficient optimizer we made up three different scenarios, which are:

- Braking on the wet concrete ($\mu_p = 0.8$)
- Braking on the wet cobblestones ($\mu_p = 0.4$)
- Surface change during braking ($\mu_p = 0.8 \to 0.4$)

In all of the scenarios a Gaussian noise is added to achieve more realistic results. For each case the friction coefficient value and wheel and vehicle velocities and they are shown in the figures.

Braking on the wet concrete ($\mu_p = 0.8$):
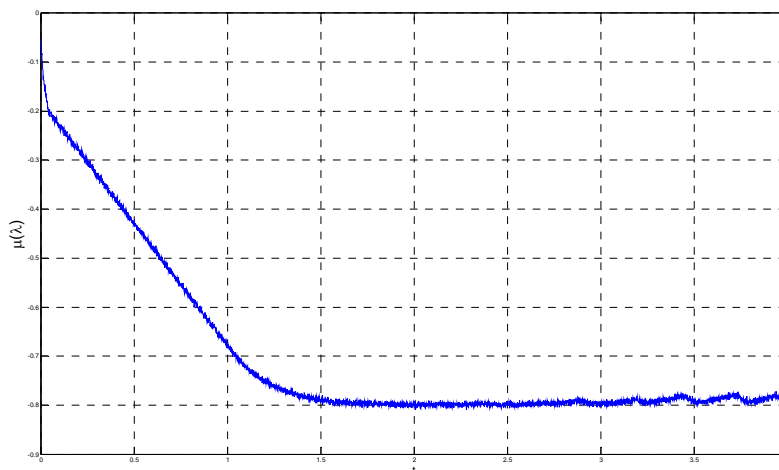
FIGURE 3.17: FRICTION COEFFICIENT (SELF OPTIMIZATION- DRY ROAD)
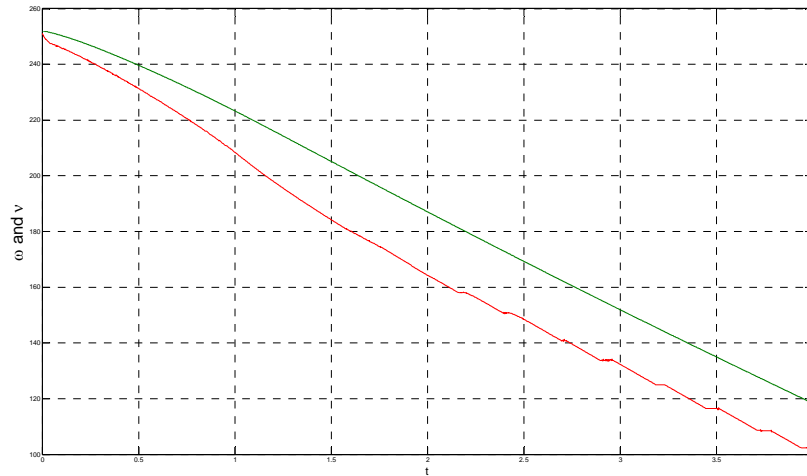
FIGURE 3.18: WHEEL AND VEHICLE VELOCITIES (SELF OPTIMIZATION- DRY ROAD)

Braking on the wet cobblestones ($\mu_p = 0.4$):
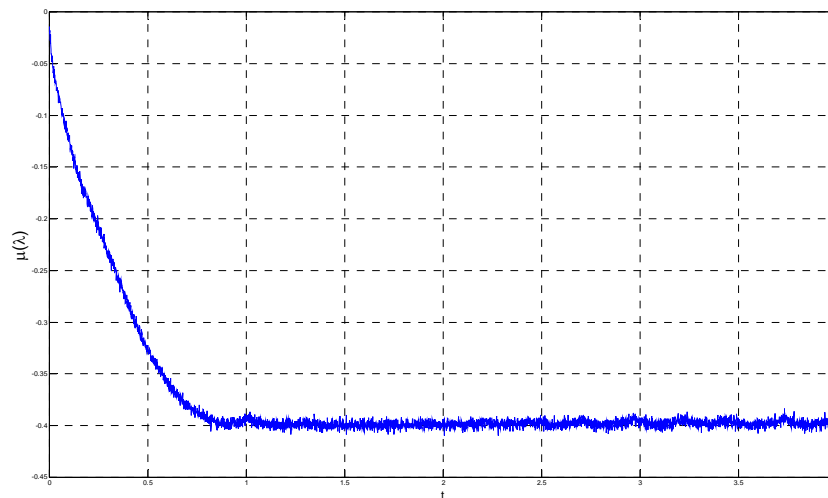
FIGURE 3.19: FRICTION COEFFICIENT (SELF OPTIMIZATION- WET ROAD)
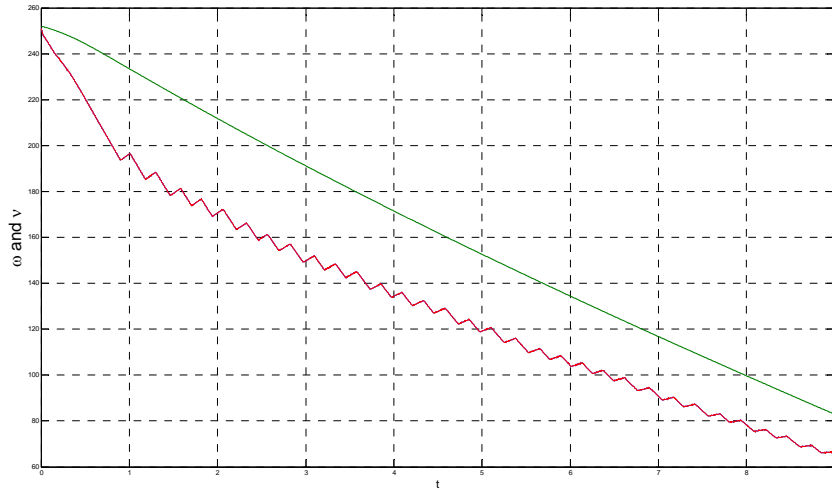
FIGURE 3.20: WHEEL AND VEHICLE VELOCITIES (SELF OPTIMIZATION- WET ROAD)

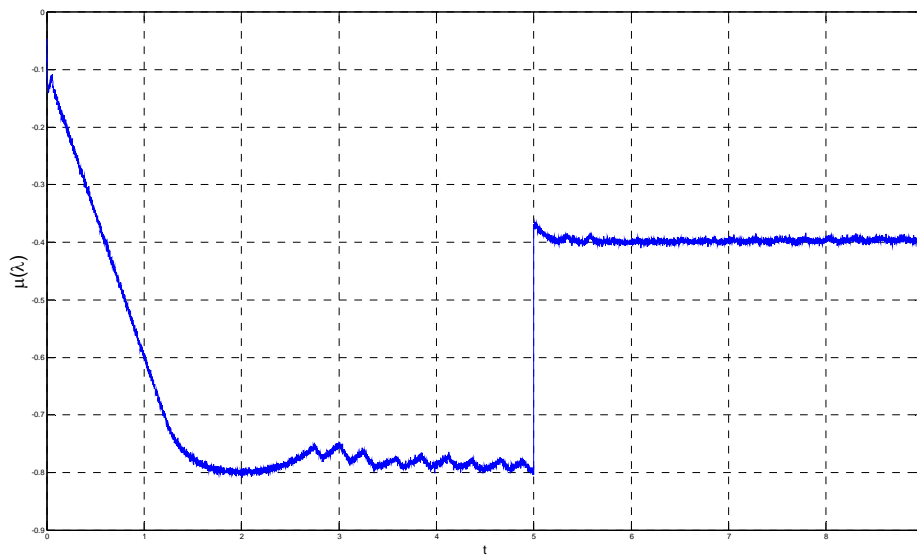_Surface change during braking_ ($\mu_p = 0.8 \rightarrow 0.4$):

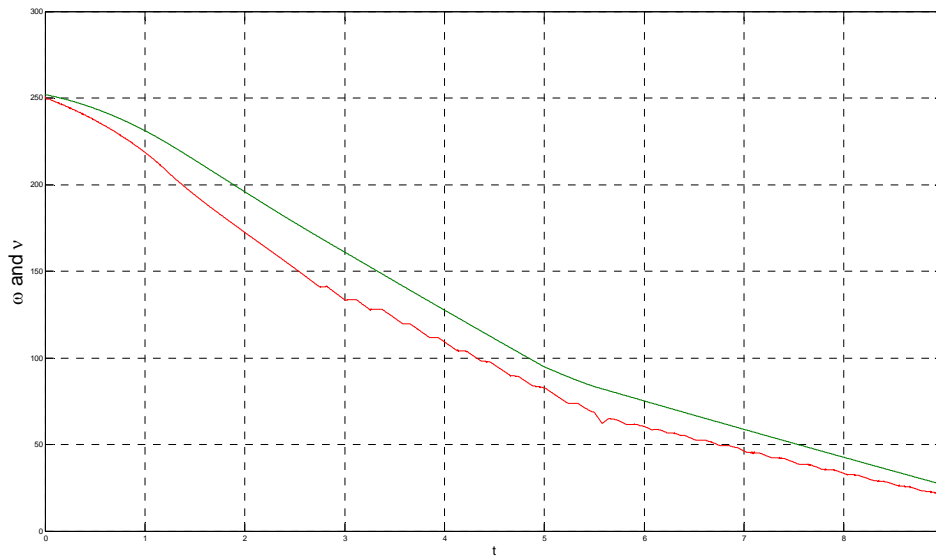FIGURE 3.21: FRICTION COEFFICIENT (SELF OPTIMIZATION- SURFACE CHANGE)

FIGURE 3.22: WHEEL AND VEHICLE VELOCITIES (SELF OPTIMIZATION- SURFACE CHANGE)

As we can see from the figures, in both of the surface conditions the controller finds the maximum friction coefficient. Also the performance of the control is very good in the surface change scenario. It immediately finds the new maximum and stays on the minimum of the friction force curve.

3.4 Friction Force Controller

Till now we have designed our wheel slip controller and the friction coefficient optimizer. The optimizer will feed the desired value to the slip controller. While the desired slip is tracked the friction force will reach to its extremum μ_p and the slip will reach to λ_p . Although this seems to be satisfactory there is a very important point that should not be missed. As we mentioned in Chapter 2 while explaining the friction characteristics of the tires, one of the biggest problems on ABS systems is the undesired slip angle or yaw moment. This can either arise from a steering input from the driver but also from the difference between the friction forces of the right and left wheels.

Imagine that you are driving on a dry asphalt road which has a μ value of 1.2 . Suddenly you apply to the brake pedal for full brake. Assume that while braking the right side of the road surface changes from dry to wet ($\mu = 0.6$) which corresponds to a change of 0.6 in the friction coefficient. This will create a yaw moment on the vehicle and the driver will lose the control of the vehicle (this case is also simulated and shown in Chapter 4). To avoid this situation a friction force controller should be implemented. The object of this controller will be to balance the friction forces between the right and left wheels, hence keeping the vehicle stable and steerable.

3.4.1 Controller Design

If we look at the dynamics of the friction force, rewriting equation 2.2 :

$$F_x = F_z \mu(\lambda, \alpha)$$

Taking the derivative of this equation under the assumption of static normal force (F_z) and zero slip angle:

$$\dot{F}_x = F_z \dot{\mu}(\lambda, \alpha) \dot{\lambda} \tag{3.30}$$

Looking at the experimental data we know that the changes in the road surface conditions are slow compared to our controller response time and they are bounded. If we assume that $\dot{\mu}(\lambda, \alpha)$ is bounded by some constant C we can rewrite the equation 3.28:

$$\dot{F}_x \leq K\dot{\lambda} \ , \ where \ K = F_z C$$

$$\dot{F_x}' = K\dot{\lambda}$$

Substituting equation 3.1 into equation 3.30 and defining f' and b' as shown we'll get the equation 3.31:

$$\dot{F_x}' = K \cdot (f + bu)$$

$$\dot{F_x}' = \underbrace{Kf}_{f'} + \underbrace{Kb}_{b'}u$$

$$\dot{F_x}' = f' + b'u \qquad (3.31)$$

Now we can see the similar behavior of the friction force dynamics with the wheel sleep dynamics. Because of this similarity, the dynamics of the friction force can be controlled in a parallel manner.

If we go through the same steps as we did for the slip control we'll come to the point that the control input is:

$$\hat{T}_t = \underbrace{-b^{-1}\left(\hat{f} - \left(\frac{\mu_d}{\hat{\mu}}\right)\dot{\lambda}_d\right)x_1}_{\hat{T}_{eq}} - \underbrace{b^{-1}Ksign(s)x_1}_{T_h} \qquad (3.32)$$

3.4.2 Simulation Results of the Friction Force Controller

In the simulations the desired friction force is selected as $F_d = -6000N$. Gaussian noise is added to the road characteristics. Two scenarios are tested for the performance calculation:

- Braking on a surface with fixed friction coefficient
- Surface change during braking

For both of the case the graphs of the friction force, the controller error and the wheel and vehicle speeds are provided.
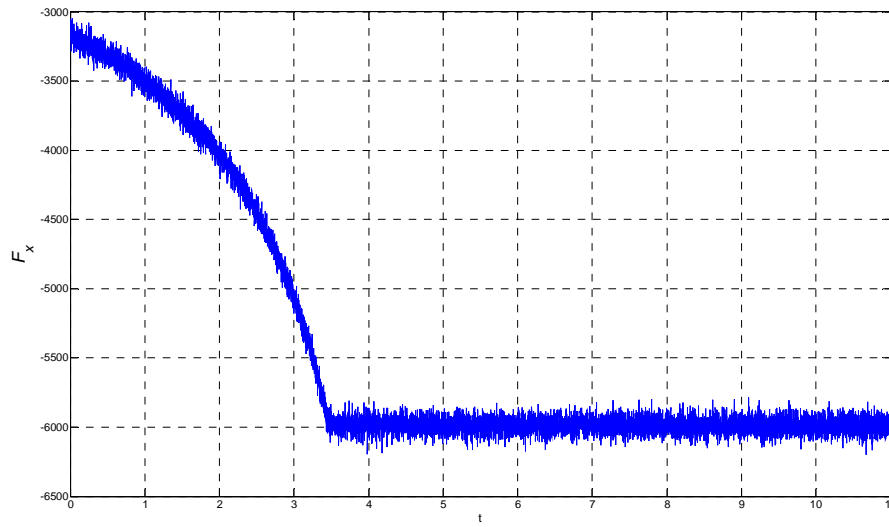
FIGURE 3.23: FRICTION FORCE (FORCE CONTROLLER- FIXED μ)
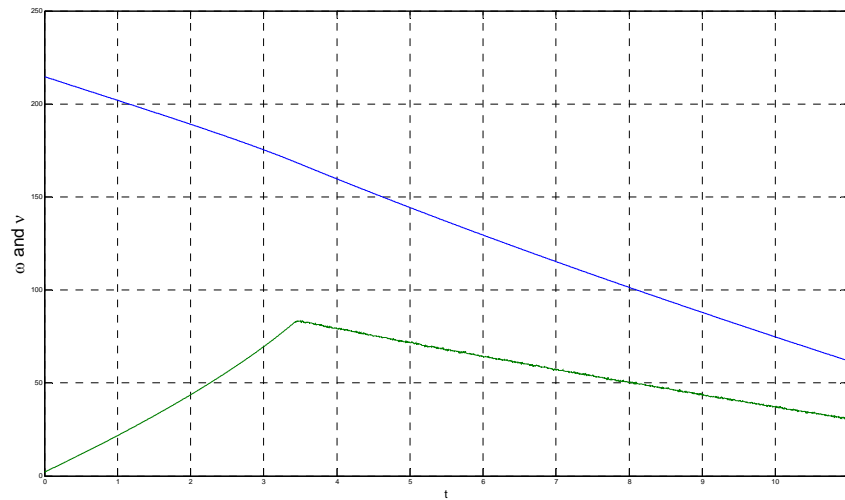
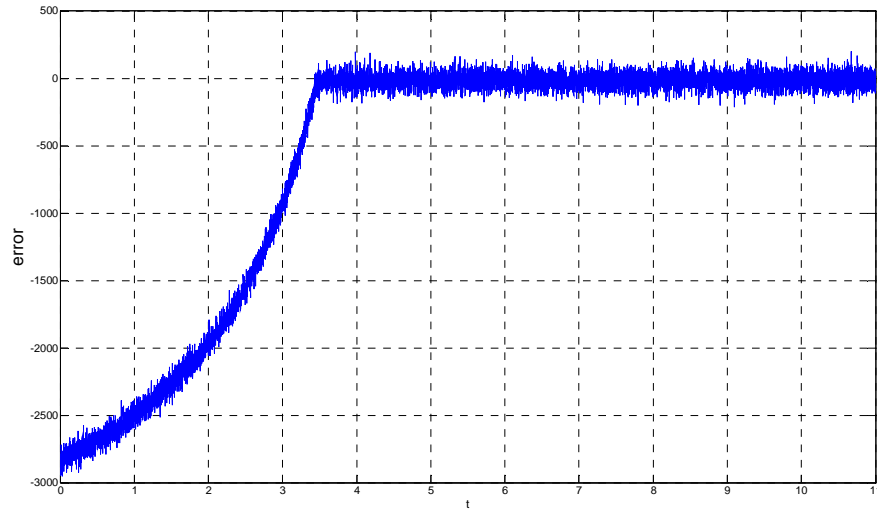FIGURE 3.24: WHEEL AND VEHICLE VELOCITIES (FORCE CONTROLLER- FIXED μ)

FIGURE 3.25: CONTROLLER ERROR (FORCE CONTROLLER- FIXED μ)
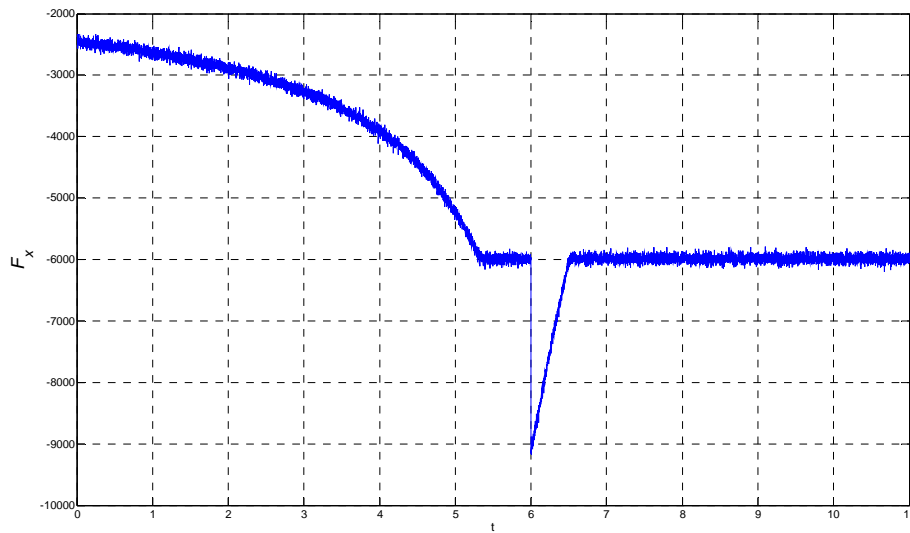
Surface change during braking:

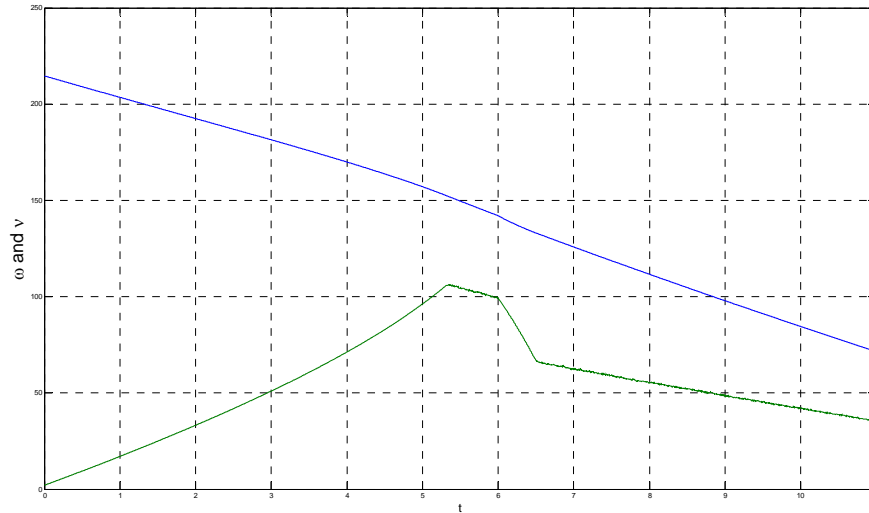FIGURE 3.26: FRICTION FORCE (FORCE CONTROLLER- SURFACE CHANGE)

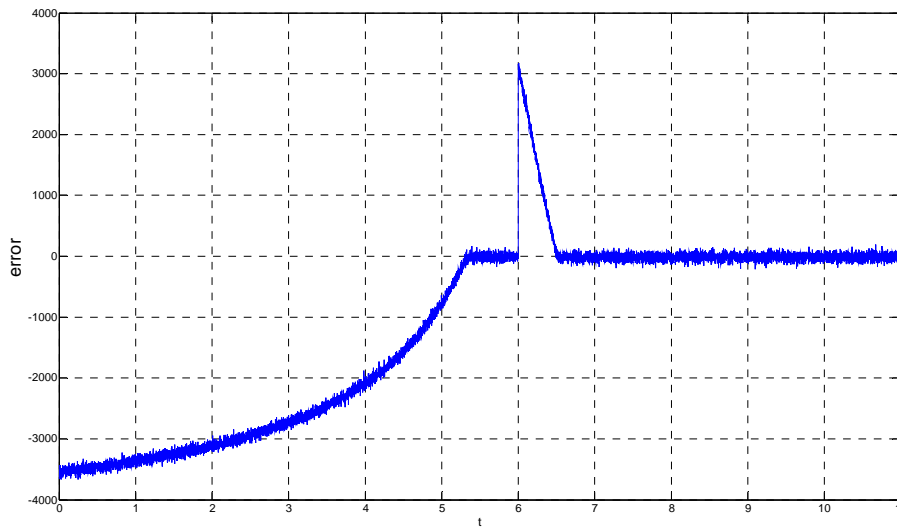FIGURE 3.27: WHEEL AND VEHICLE VELOCITIES (FORCE CONTROLLER- SURFACE CHANGE)

FIGURE 3.28: CONTROLLER ERROR (FORCE CONTROLLER- SURFACE CHANGE)

Looking at the figures in both scenarios we can say that the controller performance is satisfactory. As we mentioned in the design part, even in the surface change case the controller reaches the desired value less than a second. One difference between the results of the force controller and the slip controller is that the settling time is larger here. The reason behind this is that the initial wheel speed in force controller setup is assumed to be close to zero assuming that

44

the wheel is almost locked. As we mentioned in the simulation results of the slip controller the dynamics during the acceleration of the wheel depends on the maximum friction force. Since the initial value of the wheel speed is much smaller the settling time is larger. The simulation result with additional engine torque control is given in the figure 3.29. As we can see from the figure the settling time is less than a second.
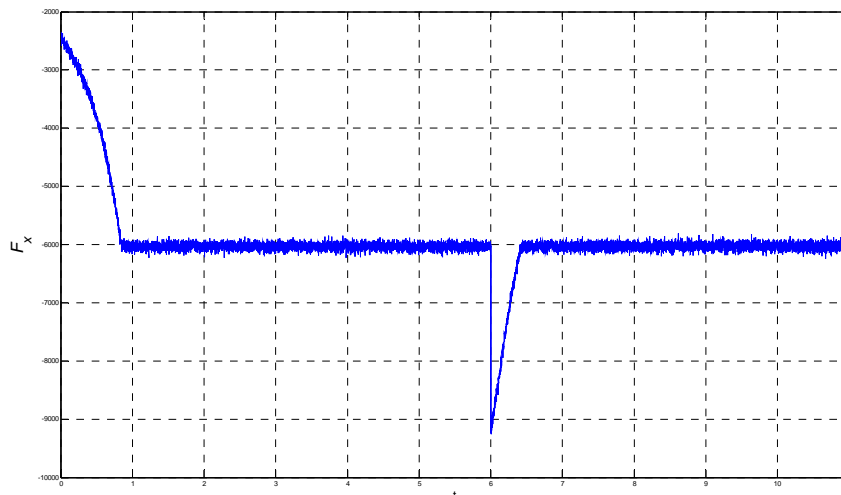

FIGURE 3.29: FRICTION FORCE (FORCE CONTROLLER- SURFACE CHANGE, WITH T$_E$)

3.5 Friction Force Observer

In all of the controllers designed previously the knowledge of the friction force of the wheel was a must. That is why in this part of this chapter we will design a SMC Friction Force observer to estimate the wheel friction force.

We will use the dynamic equation of the wheel rotational velocity which was given as:

$$\dot{\omega}_w = \frac{1}{J_w}[T_e - T_b - r_w(F_x + F_w)] \tag{2.1}$$

For simplicity we assume that the engine torque and viscous friction force are zero. If we change our equation such that:

45

$$\widehat{\dot{\omega}}_w = \frac{1}{J_w}[-T_b - r_w\, F_i] \tag{3.33}$$

where,

$F_i = Hsign(\bar{\omega}_w)$, and $\bar{\omega}_w = (\omega_w - \widehat{\omega}_w)$ is the estimation error of ω_w.

Choosing our sliding surface to be:

$$s = \bar{\omega}_w = (\omega_w - \widehat{\omega}_w) \tag{3.34}$$

Taking the derivative of equation 3.34 and substituting equations 2.1 and 3.33 to find the error dynamics:

$$\dot{s} = -F_x - Hsign(s) \tag{3.35}$$

From the previous chapter we know that the stability criteria for this controller can be found by the equation:

$$s\dot{s} \leq 0 \tag{3.10}$$

Substituting equation 3.35 into 3.10, we get :

$$-sF_x - H|s| \leq 0 \tag{3.36}$$

$$H > |F_x| \tag{3.37}$$

Equation 3.37 is the convergence constraint for the observer. Again to avoid chattering the signum function can be replaced with the saturation function.

To obtain the equivalent value of the estimated friction force we use a low pass filtering of the form:

$$W(s) = \frac{1}{Ds + 1}$$

where D is the cut-off frequency of the filter.

3.5.1 Simulation Results of the Friction Force Observer

The simulation results of the friction force observer are given below. The simulation setup is the same as the desired slip tracking simulation. D value is set to 0.03 and H is set to 10^4.
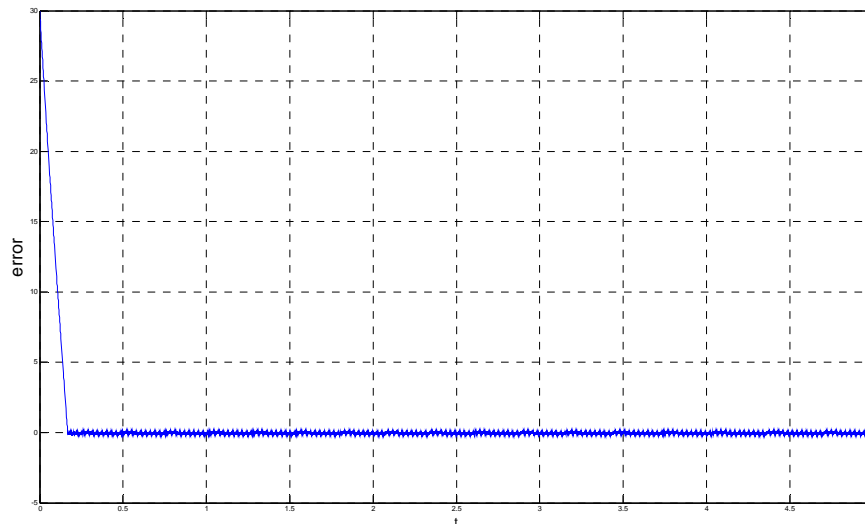
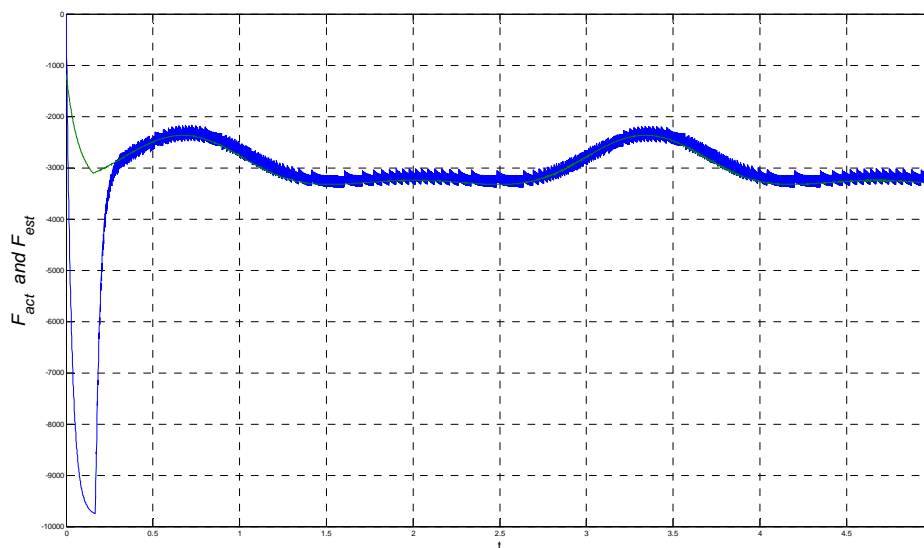

FIGURE 3.30: OBSERVER ERROR (FRICTION FORCE OBSERVER)

FIGURE 3.31: ACTUAL AND ESTIMATED FRICTION FORCE (FRICTION FORCE OBSERVER)

The results of the observer are satisfactory. The error decays less than a half second.

3.6 Merging All of the Controllers

Finally we can combine all the controllers designed previously to build the overall ABS controller. We know that the self optimizer and the slip controller pair will do the maximization of the friction force. The friction force controller will balance the friction forces between left and right wheels when there is a large difference in friction forces. This means that we have actually two controllers to switch in between.

Defining a simple relay controller, which will switch between these two controllers, seems to be able to handle this job.

For any right and left wheel couples the overall control system is given in Figure 3.32.

If $F_r > F_l + \Delta$ then the friction force controller for the right wheel is activated ;
else the self optimization contoller is activated .

If $F_l > F_r + \Delta$ then the friction force controller for the left wheel is activated ;
else the self optimization contoller is activated .

Where Δ is the treshold value.

To avoid high frequency switching hysteresis can be added to the relay element.
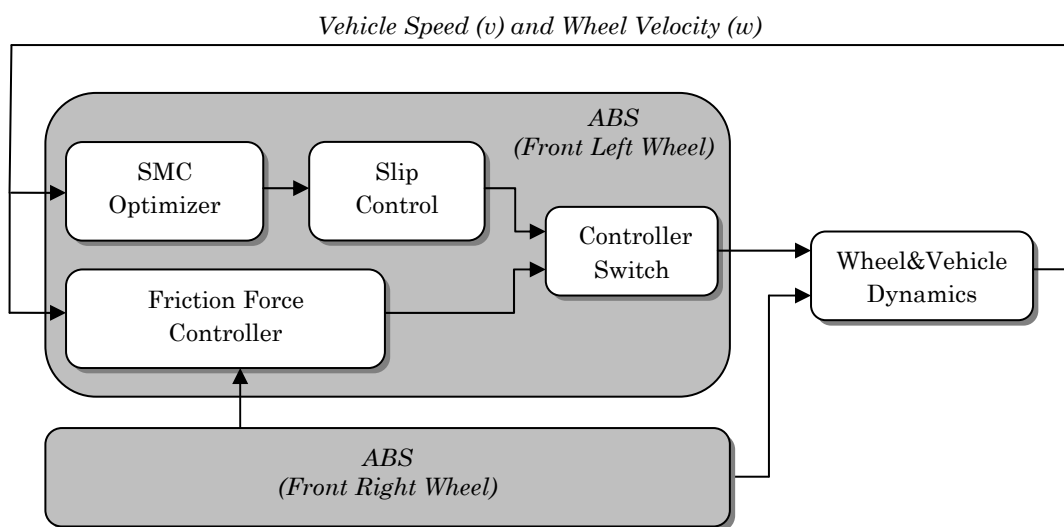
FIGURE 3.32: ABS CONTROL BLOCK DIAGRAM FOR THE FRONT LEFT WHEEL.

3.6.1 Simulation Results of the Overall System

To be able to see the full performance of the Overall System we created the following scenario:

- Driving speed of the car at $t = 0$ is $v = 250 km/h$ and the slip values of each wheel is $\lambda = 0$. All of the wheels are on the same road surface with $\mu_p = 0.8, \lambda_p = 0.12$.
- Full brake is applied at $t = 0$.
- During braking at $t = 5\ and\ t = 5.5$ the front left and the rear left wheels enter a road surface with $\mu_p = 0.4, \lambda_p = 0.19$ while the right wheels continue their motion on the surface with $\mu_p = 0.8$.

What we expect to see here is that all of the optimization controllers are activated reaching $\mu_p = 0.8$ for each wheel at first. At $t = 5$ since the front left wheel enters the slippery surface, the optimization controller should reach the new friction coefficient value which is $\mu_p = 0.4$. The transition to the slippery surface halves the left wheel friction force; hence the right wheel should switch from the optimizer to the friction force follower mode and lower its friction force to the same value. The same actions should also be taken by the controllers of the rear wheels. The following figures show the wheel and vehicle velocities, the friction force coefficients, friction force differences and the yaw angle. (Since the response of the rear wheels is just the delayed version of the front wheels only the friction coefficient and the friction force difference results of the front wheel pair are shown)
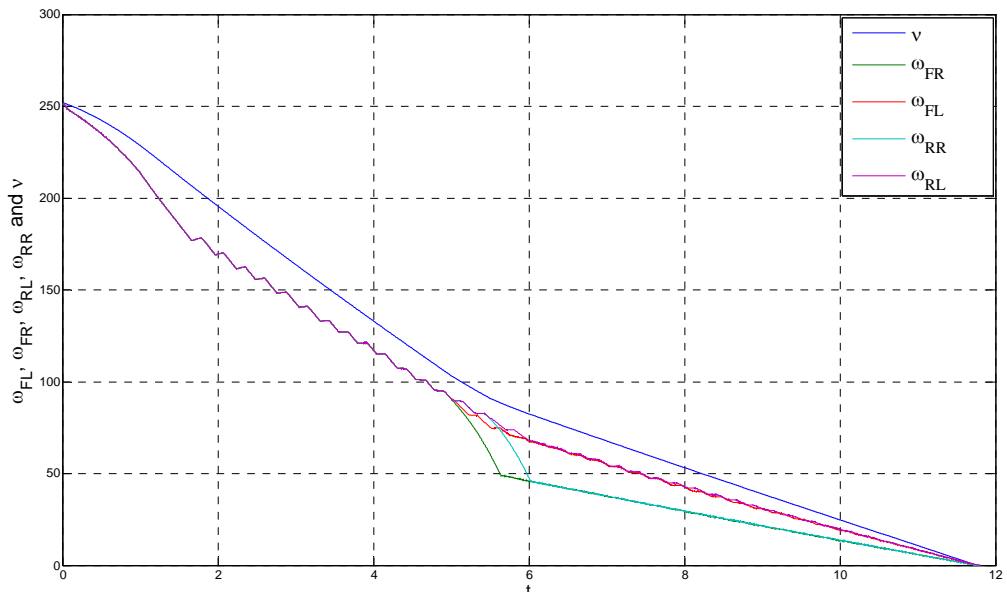
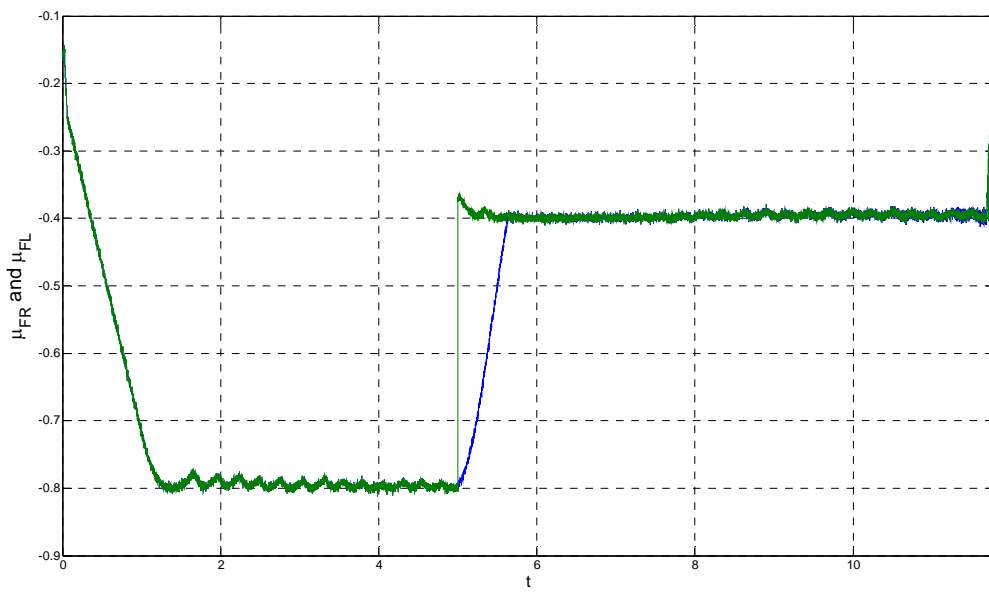FIGURE 3.33: WHEEL AND VEHICLE VELOCITIES (OVERALL SYSTEM)

FIGURE 3.34: FRICTION FORCE COEFFICIENTS μ_{FL} AND μ_{FR} (OVERALL SYSTEM)
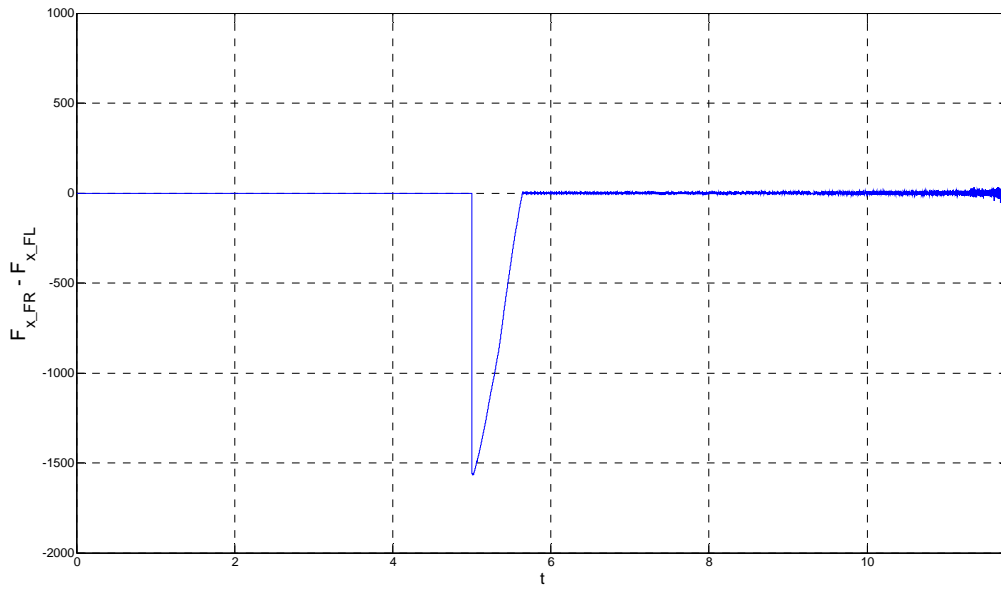
FIGURE 3.35: FRICTION FORCE DISTANCE ($F_{x_{FR}} - F_{x_{FL}}$) (OVERALL SYSTEM)
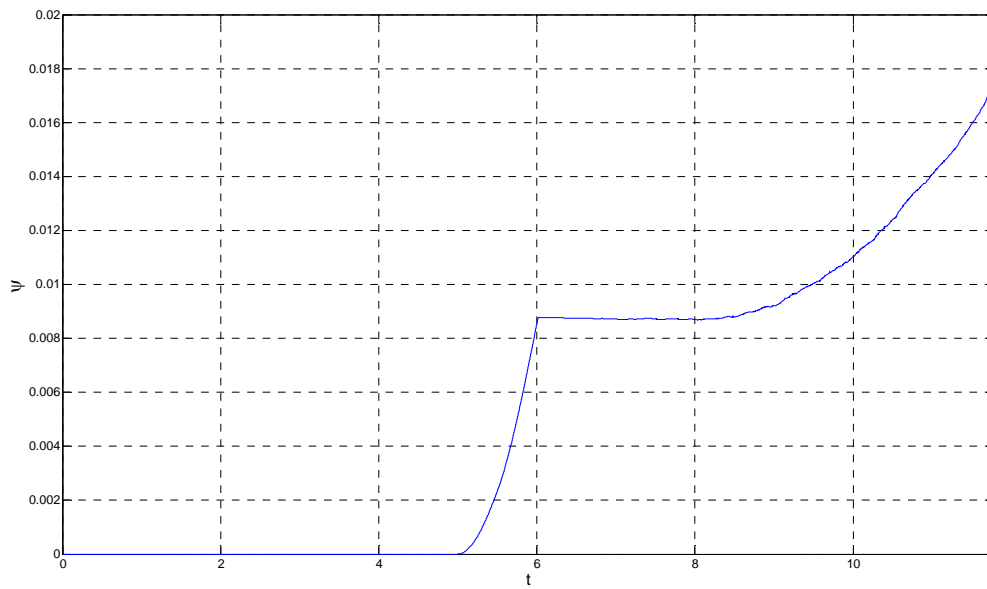

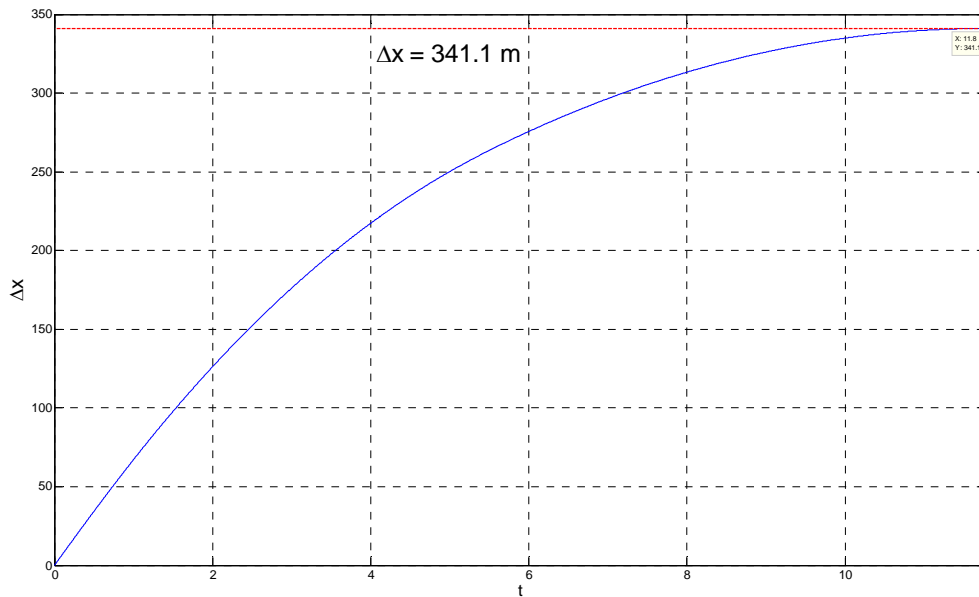FIGURE 3.36: YAW ANGLE (ψ) (OVERALL SYSTEM)

51

FIGURE 3.37: BRAKING DISTANCE (OVERALL SYSTEM)

As we can see from the figures the system acts as expected. The initially all the wheels set their slip values such that the friction force is maximized. When the left wheels enter the slippery surface the right wheel controllers change their slip values such that the friction forces are balanced hence the stability of the vehicle is preserved. If we look at the Figure 3.33 we can see the consecutive change in the slip values of the front right and rear right wheels in the time period t=(5, 6)sec. In Figure 3.36 the final yaw angle is shown which has a value of 0.0182°. This value tells us that the deviation from the original route is almost 0, hence the stability is preserved.

Now let us repeat the same maneuver is without ABS to see the performance of the system more clearly. The main performance criteria's for the ABS are:

- Braking distance
- Stability of the vehicle (yaw angle)
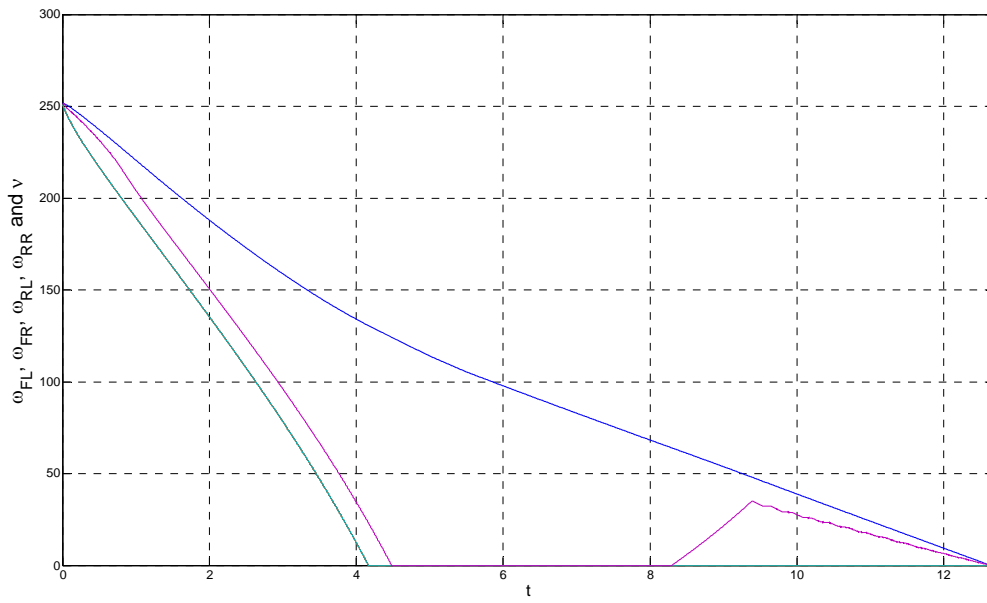
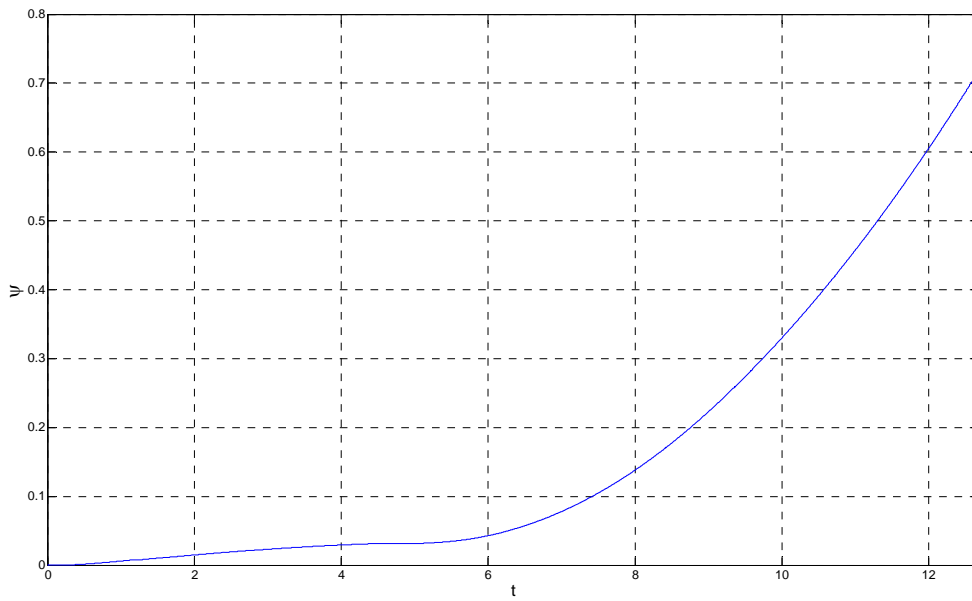FIGURE 3.38: WHEEL AND VEHICLE VELOCITIES (W/O ABS)
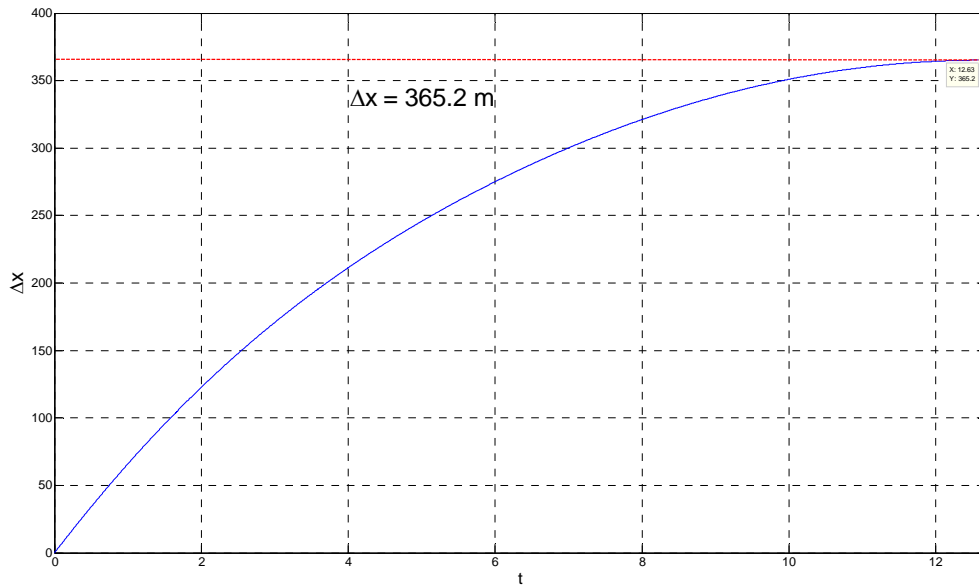

FIGURE 3.39: YAW ANGLE (ψ) (W/O ABS)

FIGURE 3.40: BRAKING DISTANCE (W/O ABS)

If we look at the Figure 3.38 we can see that all of the wheels are locked after t=4 sec. Although one of them start to rotate after t=8 sec the rest remains locked till the vehicle stops. This sets their friction coefficient values to -1 which provides less friction force, hence a longer braking distance. In Figure 3.40 the braking distance is shown where $\Delta x = 365.2m$. If we compare this result with the one shown in Figure 3.37 where ABS is active we can see that the difference is $24.1m$ which is considerable (corresponding to 6.6% better performance).

For considering the stability of the ABS we can look at the Figures 3.36 and 3.39. While in the second simulation where the vehicle w/o ABS the yaw angle after braking is 0.7° in the first simulation this value is 0.018°.

4 Experimental Results

In this chapter we explain the experimental setup and give a short introduction to the CarMaker software at first. Then the driving scenarios and the performance criteria's are briefly described. This is followed by the results for each scenario. After the conclusions we'll finish the chapter with the possible future work.

4.1 Experimental Setup

The proposed ABS model is tested on the CarMaker, a vehicle dynamics and driving simulation software from the IPG Automotive Company.

IPG Automotive was founded in 1984 as a spin-off of Karlsruhe University. Since then, they have been developing vehicle dynamics and driving simulators. They hold seminars and attend to automotive conferences each year. Their products are well known and as a company they are worldwide respected. They work with almost all of the world leading automotive companies. Some of them are DaimlerChrysler, BMW, Audi, Porche, Opel, Nissan, Ford, General Motors, Renault, Pegeout, Siemens, Smart, Continental, Wabco, etc... and many more. More information on the company profile can be obtained from their website.

Their main product CarMaker is based on a well aligned simulation environment with Flex4Net technology and allows the model based testing and development of entire vehicles, vehicle components and ECUs. Its application areas are: "Classical Vehicle Dynamics", "Control Systems", "Driver Assistance Systems", "Integrated Vehicle Dynamics" and "Hybrid and Consumption".

We are using the controls and vehicle dynamics part of the program in our simulations. It is a very flexible and realistic program where we can implement our control algorithms developed in Matlab/Simulink into the CarMaker model and simulate. We can also define the driving conditions including the road, vehicle, driver models according to our needs which enable us to test very extreme conditions.

4.2 Simulation Scenarios:

The ABS model is tested in several scenarios. Each scenario is specified with the following parameter: the friction coefficient of the right and left lanes during braking. It is well-known that the performance of a vehicle even with a conventional ABS system is much better than a vehicle w/o ABS. That is why we are going to compare the SMC ABS with the conventional ABS that comes with the CarMaker as a built-in system. Our performance criteria are:

- Braking Distance
- Yaw Angle

The following scenarios are created in the program and their results are given:

- Scenario I: Both wheels are on high friction surface with $\mu_p = 0.8$, full brake is applied.
- Scenario II: Both wheels are initially on high friction surface ($\mu_p = 0.8$), full brake is applied. During braking the vehicle enters a low friction surface ($\mu_p = 0.4$) with both sides.
- Scenario III: Initially the left side of the vehicle is on low friction surface ($\mu_p = 0.4$) and the right side is on high friction surface ($\mu_p = 0.8$), full brake is applied. During braking the left side enters a lower friction surface ($\mu_p = 0.2$).
- Scenario IV: Initially both wheels are initially on high friction surface ($\mu_p = 0.8$), full brake is applied. During braking left side of the vehicle enters a low friction surface ($\mu_p = 0.6$) at first. Then the right side of the vehicle enters a lower friction surface ($\mu_p = 0.2$). Then the left side goes on a high friction surface ($\mu_p = 0.8$). Finally the right side also enters the high friction region and the vehicle stops.

In all of the scenarios the vehicle speed is initially 150km/h. The test vehicle is the VW Beetle. The vehicle is loaded with 2 passengers of weight 70kg in the

first three scenarios and the 2 passengers with 70kg plus 2 passengers with 50kg weight in the last scenario. In the first three scenarios the driver is able to turn the steering wheel more than 360°. The last scenario is repeated for two steering availability values (360° and 50°(limited case)) to see the stability performance more clearly.

The following figures are presented for the scenarios:

- Friction forces on all wheels
- Wheel and vehicle speeds
- Braking distance value
- Yaw angle value (scenarios III&IV only)

Also the simulation videos and all the Matlab/Simulink models are stored in a CD and attached to the thesis.

4.2.1 Scenario I:

Conventional ABS:

The braking distance value : **157.18m**
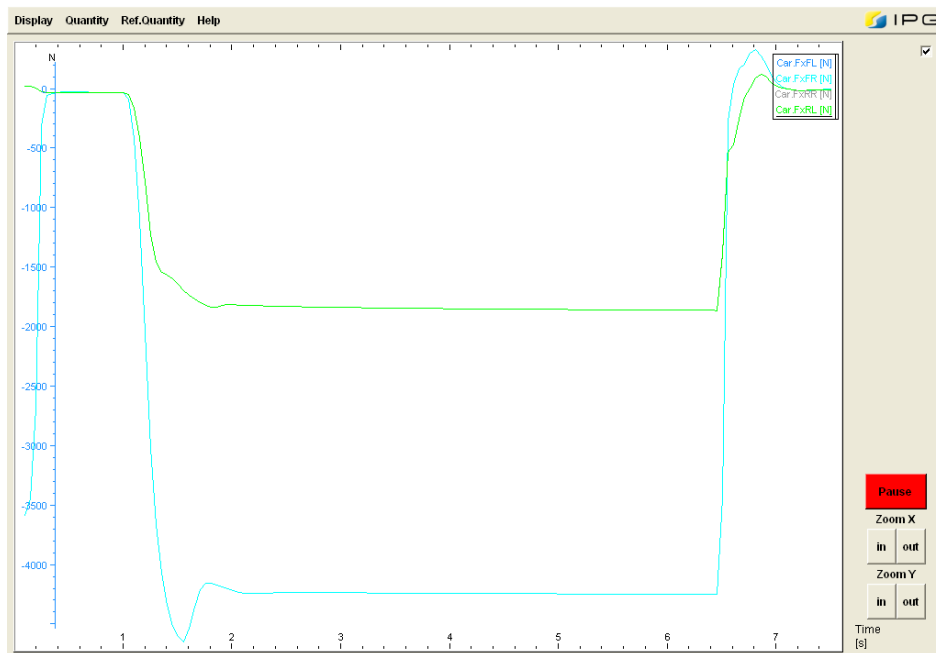
FIGURE 4.1: FRICTION FORCES (SCENARIO I, STD-ABS)
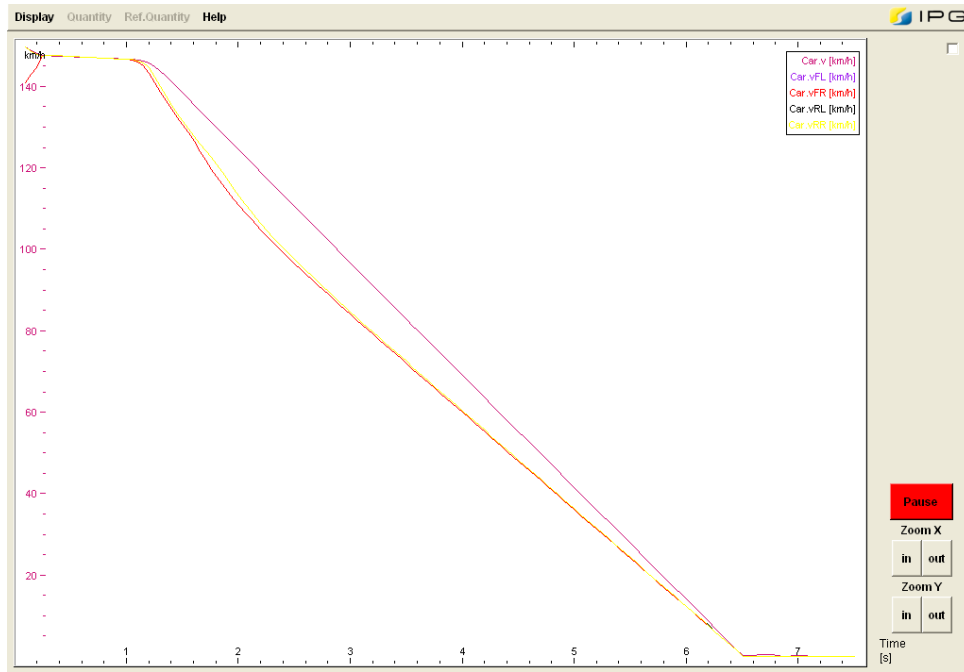
FIGURE 4.2: WHEEL & VEHICLE VELOCITIES (SCENARIO I, STD-ABS)

SMC-ABS:

The braking distance value : **148.51m**
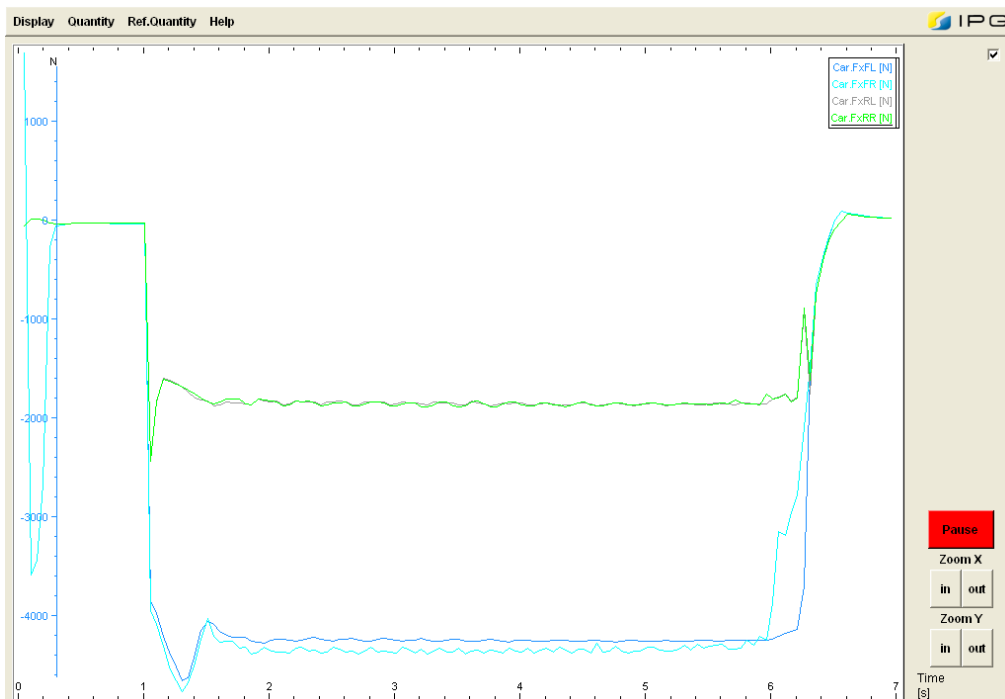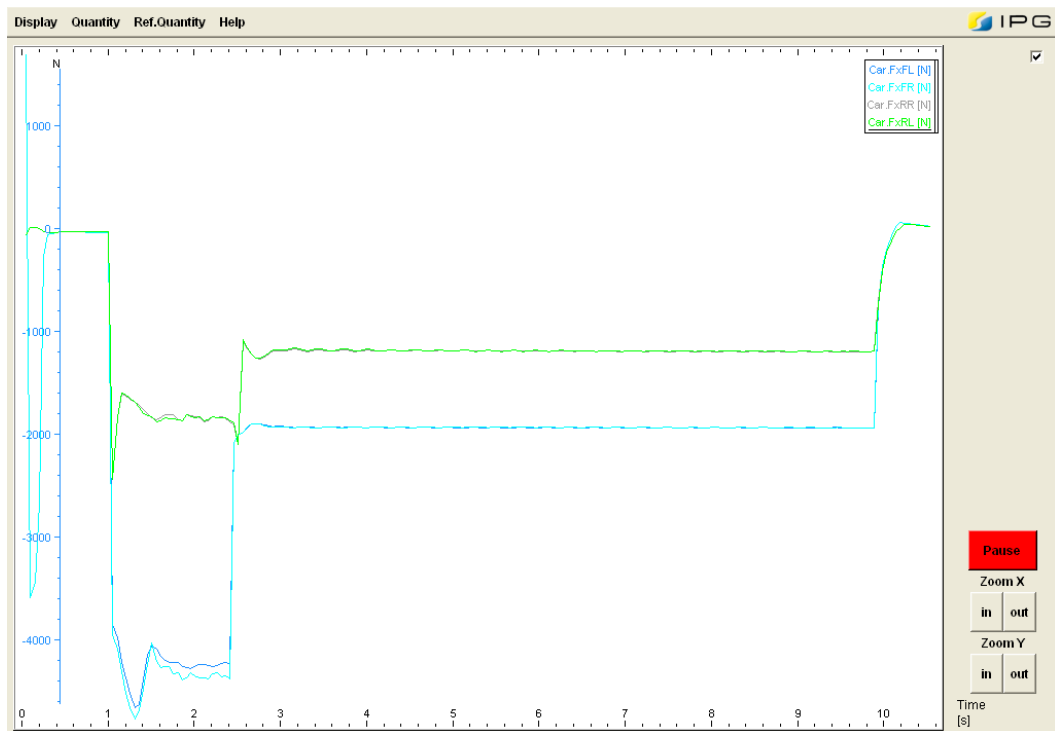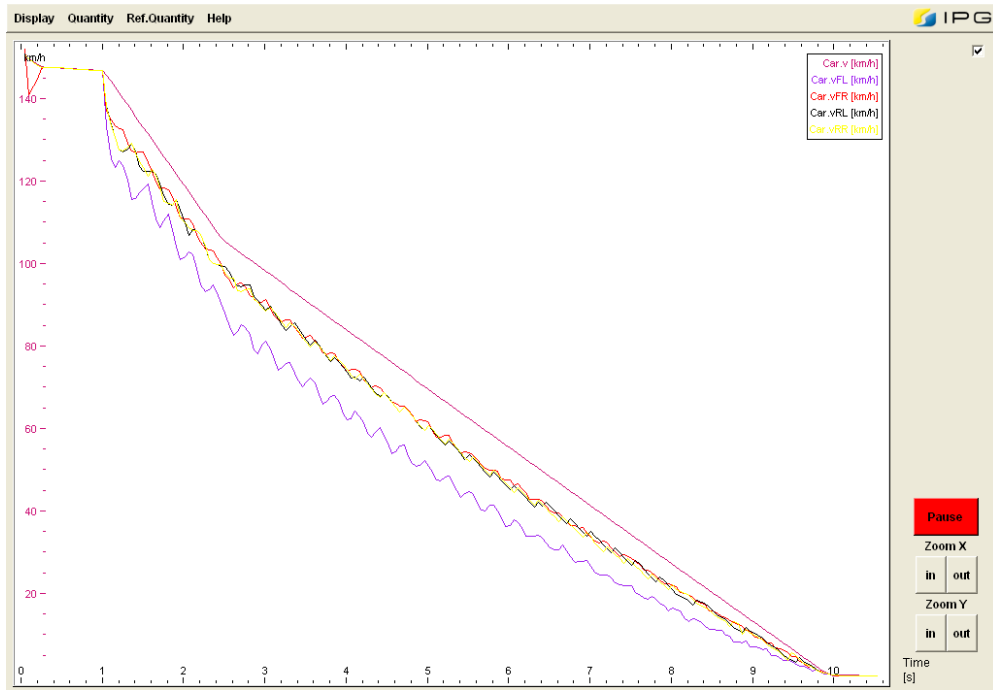

FIGURE 4.3: FRICTION FORCES (SCENARIO I, SMC-ABS)
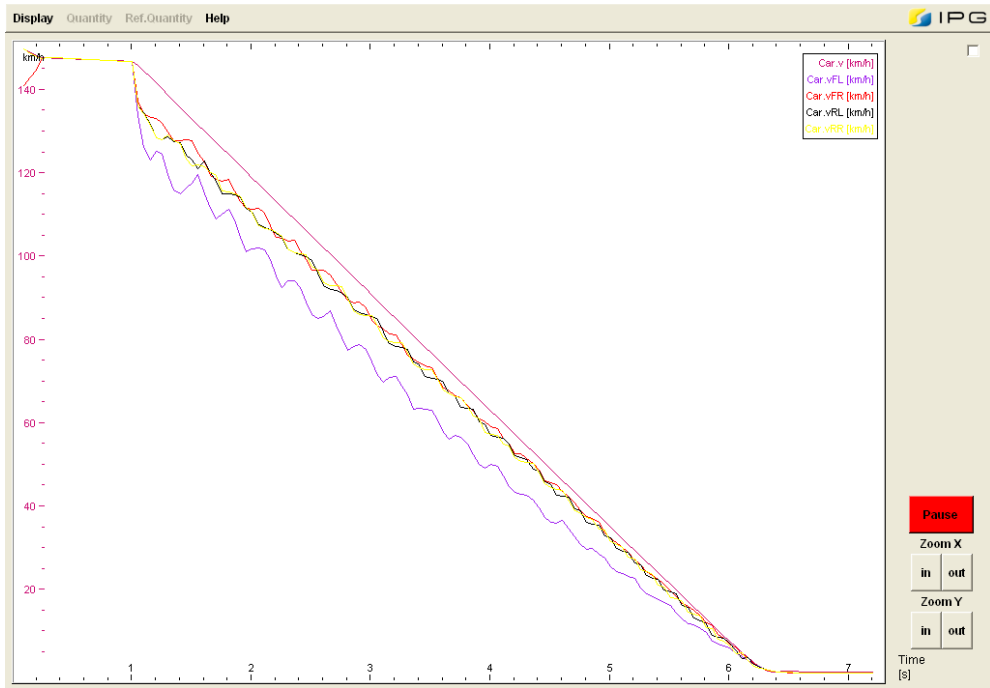
FIGURE 4.4: WHEEL & VEHICLE VELOCITIES (SCENARIO I, SMC-ABS)

4.2.2 Scenario II:

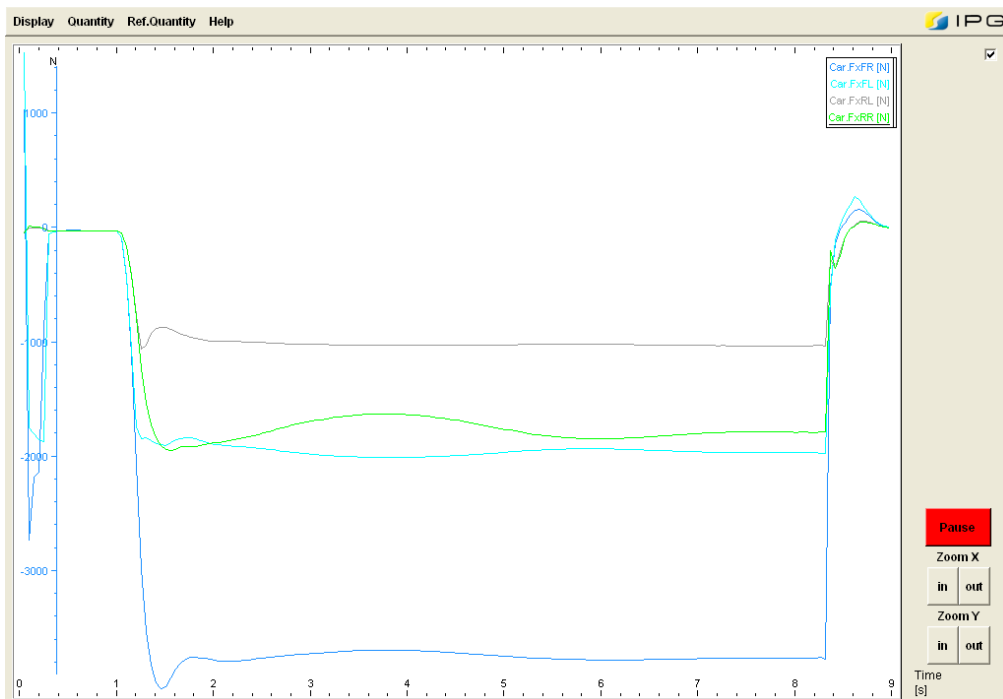*Conventional ABS:*

The braking distance value : **217.57m**
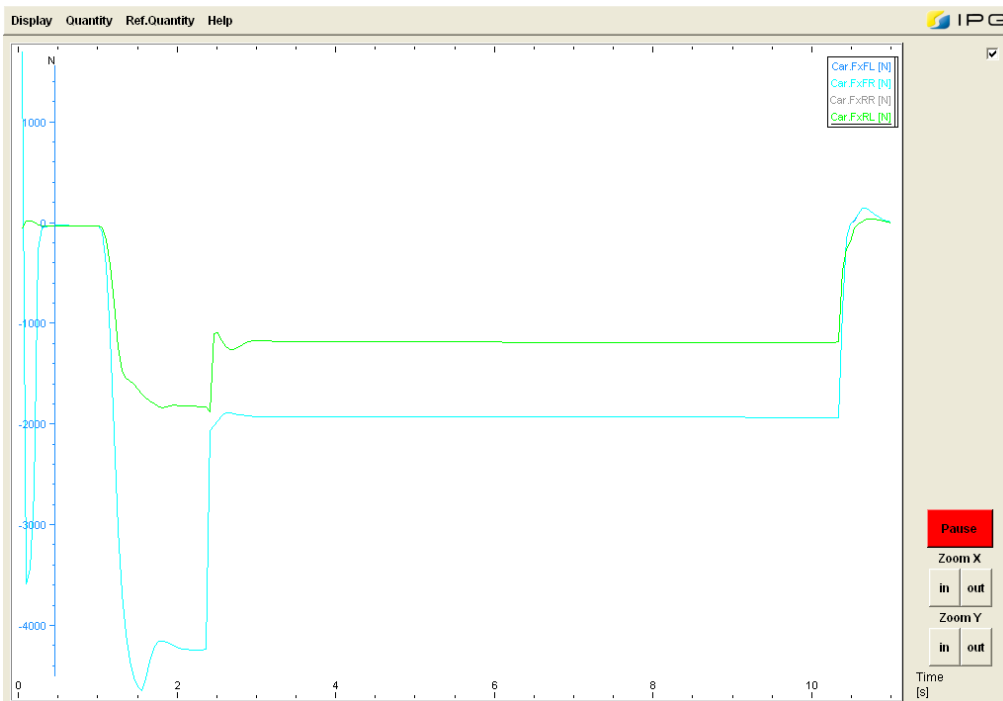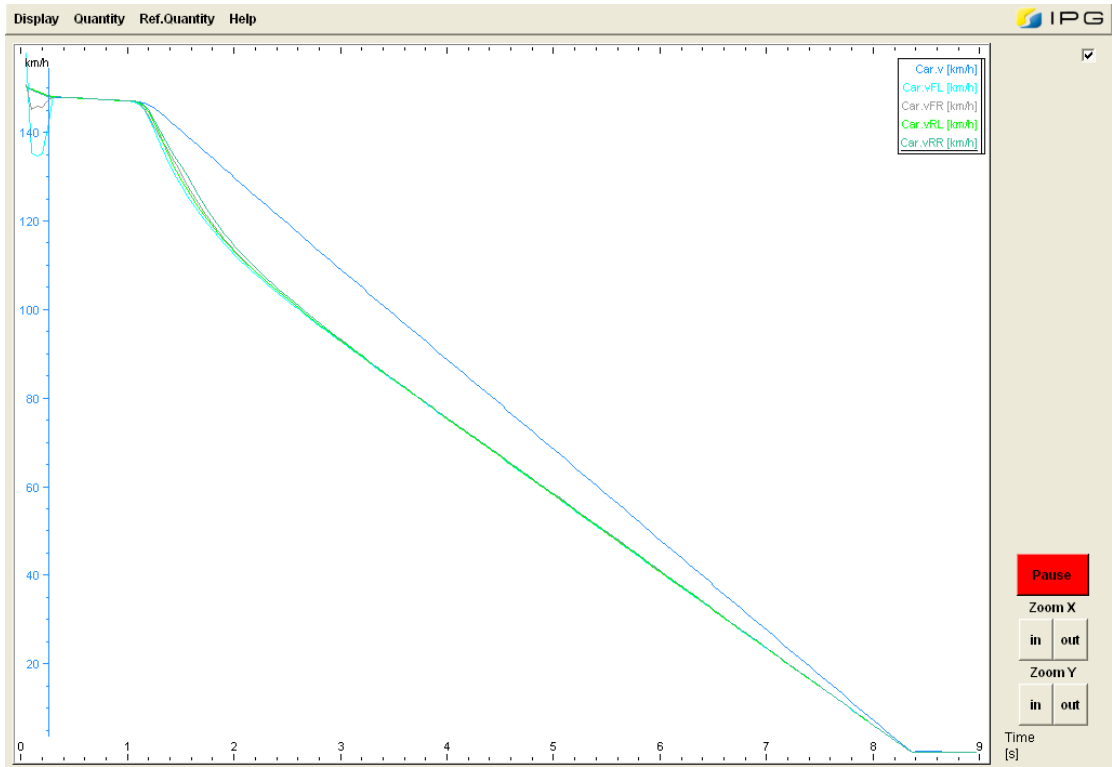

FIGURE 4.5: FRICTION FORCES (SCENARIO II, STD-ABS)
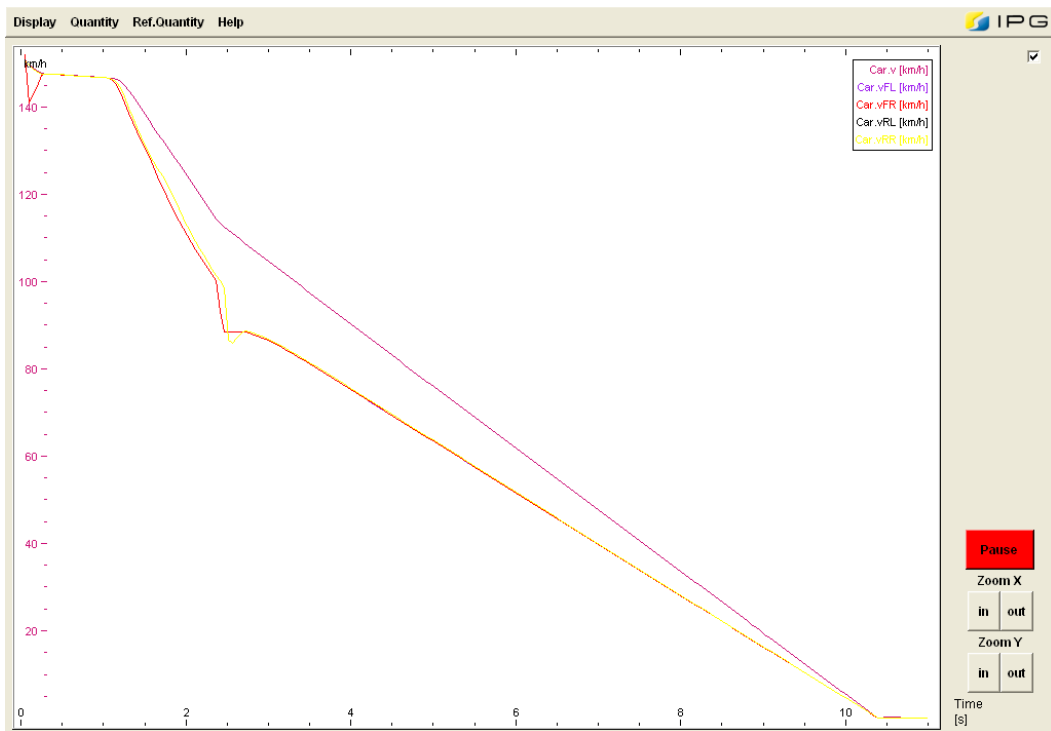
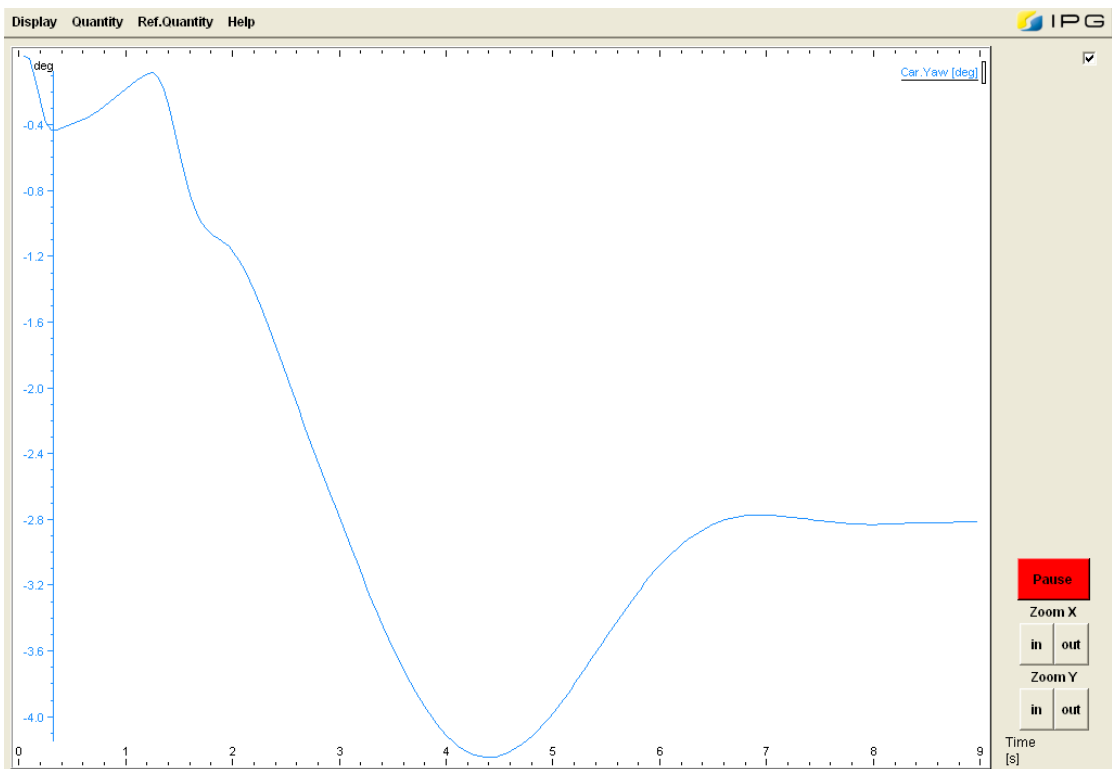FIGURE 4.6: WHEEL & VEHICLE VELOCITIES (SCENARIO II, STD-ABS)

<u>*SMC-ABS:*</u>

The braking distance value : **202.4m**

FIGURE 4.7: FRICTION FORCES (SCENARIO II, SMC-ABS)

60

FIGURE 4.8: WHEEL & VEHICLE VELOCITIES (SCENARIO II, SMC-ABS)

4.2.3 ScenarioIII:

Conventional ABS:

The braking distance value : **217.95m**

FIGURE 4.9: FRICTION FORCES (SCENARIO III, STD-ABS)

FIGURE 4.10: WHEEL & VEHICLE VELOCITIES (SCENARIO III, STD-ABS)

FIGURE 4.11: YAW ANGLE (SCENARIO III, STD-ABS)

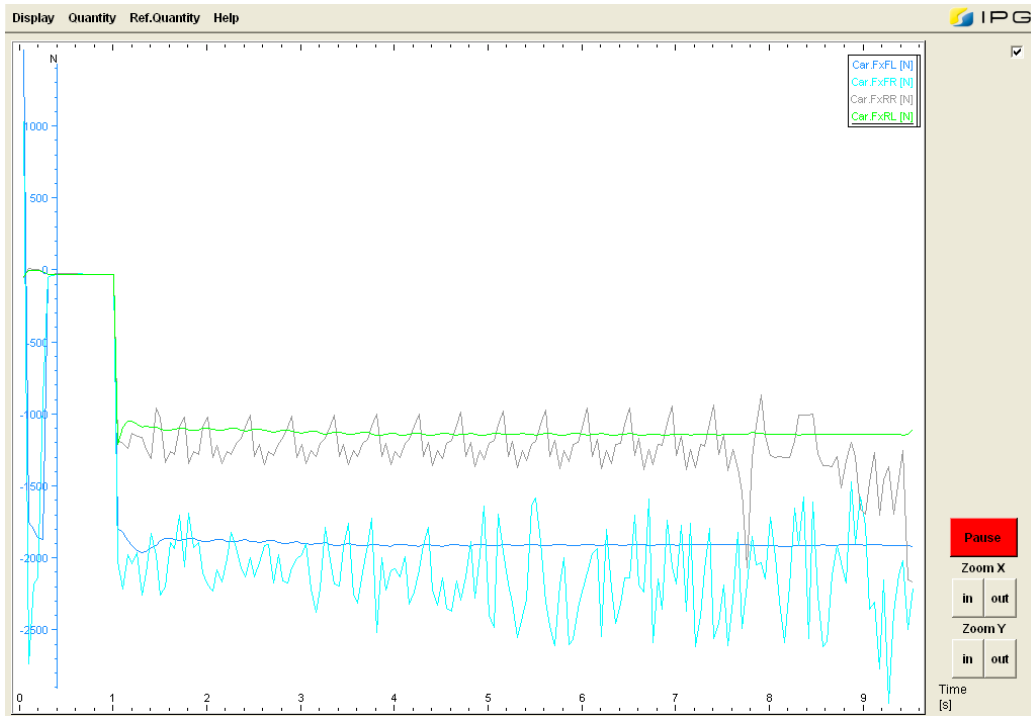_SMC-ABS:_

The braking distance value : **289.18m**

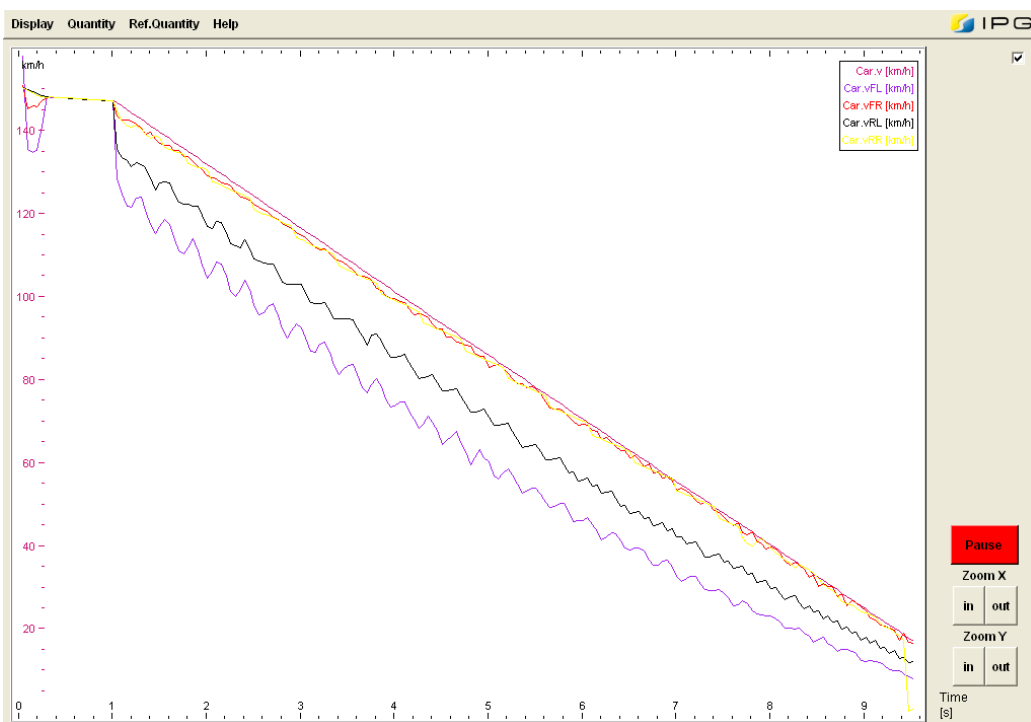
FIGURE 4.12: FRICTION FORCES (SCENARIO III, SMC-ABS)

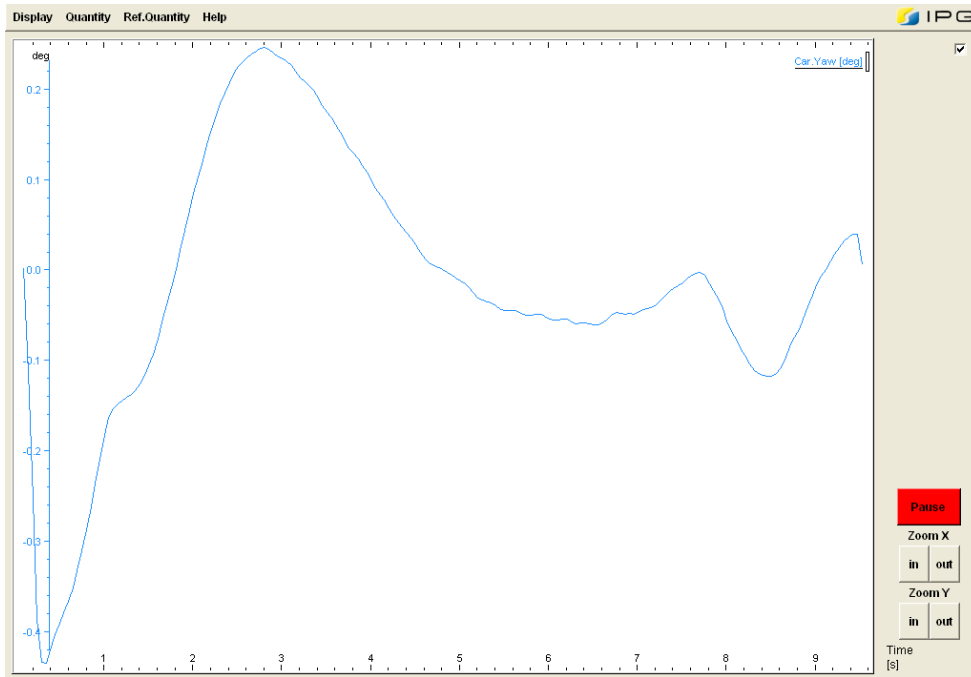FIGURE 4.13: WHEEL & VEHICLE VELOCITIES (SCENARIO III, SMC-ABS)

FIGURE 4.14: YAW ANGLE (SCENARIO III, SMC-ABS)

4.2.4 Scenario IV:

4.2.4.1 Steer ability: 360°
<u>Conventional ABS:</u>

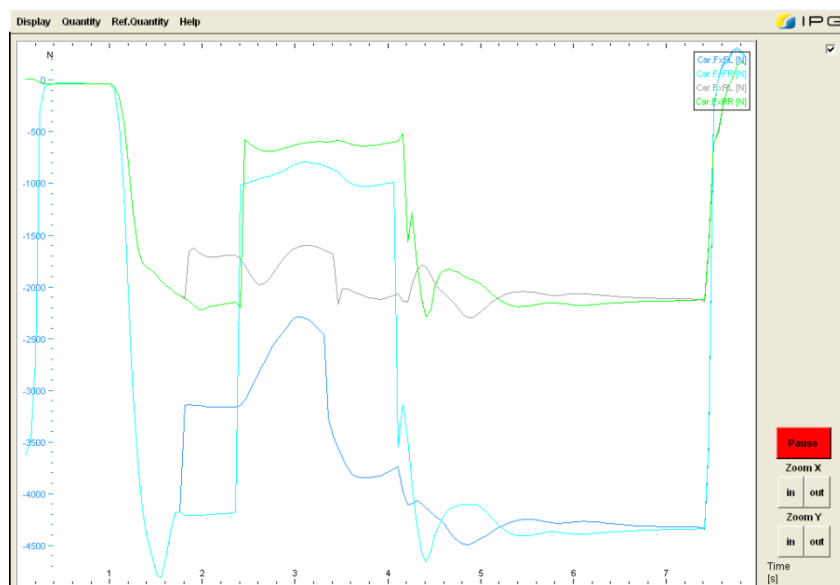The braking distance value : **217.95m**

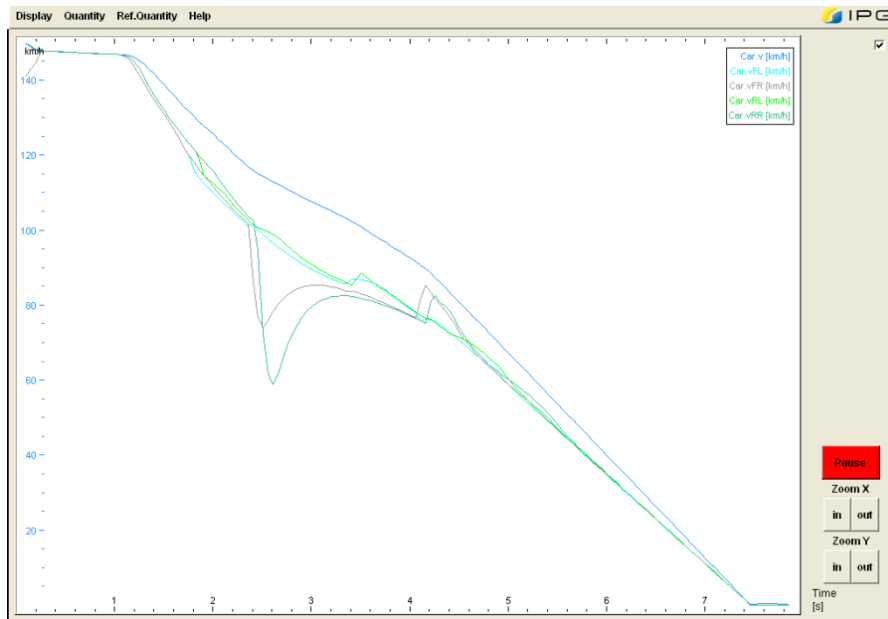

FIGURE 4.15: FRICTION FORCES (SCENARIO IV, STD-ABS, 360°)

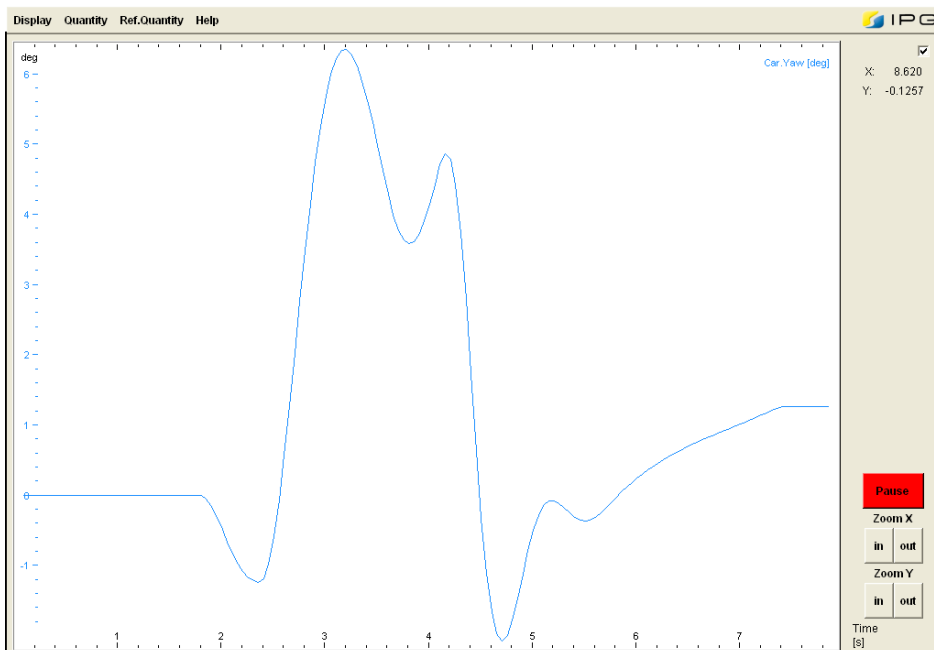FIGURE 4.16: WHEEL & VEHICLE VELOCITIES (SCENARIO IV, STD-ABS, 360°)

FIGURE 4.17: YAW ANGLE (SCENARIO IV, STD-ABS, 360°)

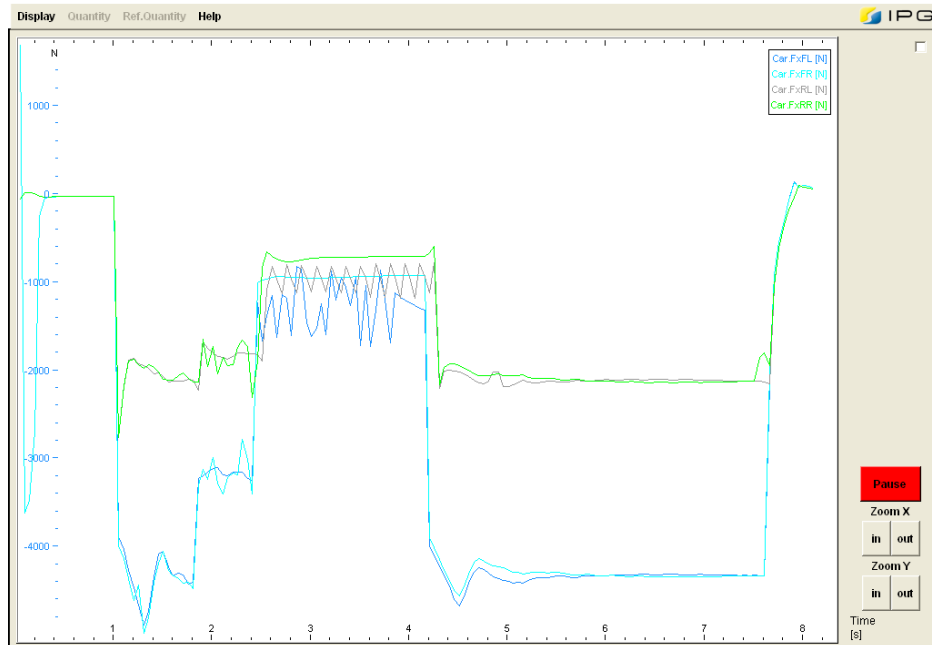The braking distance value : **289.18m**

FIGURE 4.18 FRICTION FORCES (SCENARIO IV, SMC-ABS, 360°)

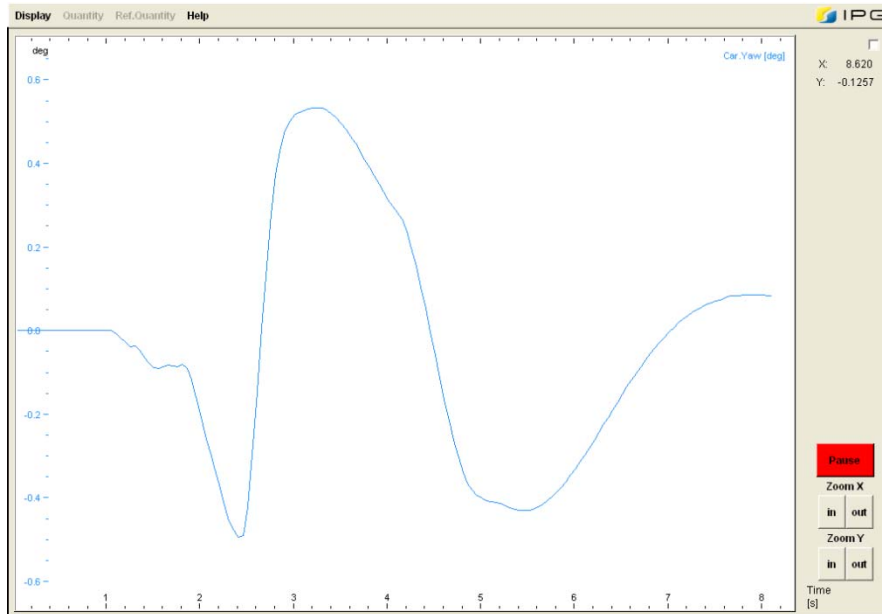FIGURE 4.19: WHEEL & VEHICLE VELOCITIES (SCENARIO IV, SMC-ABS, 360°)

FIGURE 4.20: YAW ANGLE (SCENARIO IV, SMC-ABS, 360°)

4.2.4.2 Steer ability: 50°

Conventional ABS:

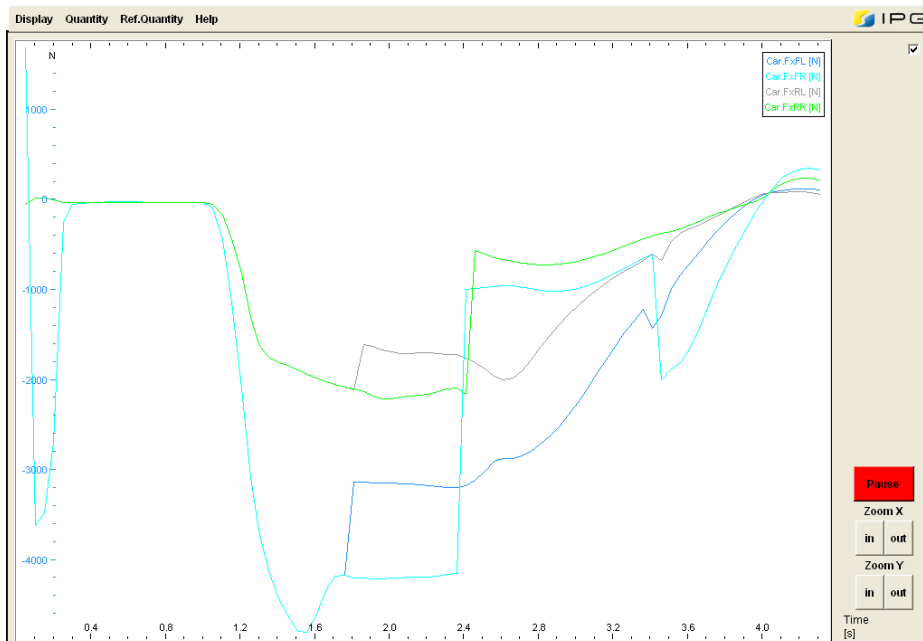The braking distance value : **217.95m**

FIGURE 4.21 FRICTION FORCES (SCENARIO IV, STD-ABS, 50°)
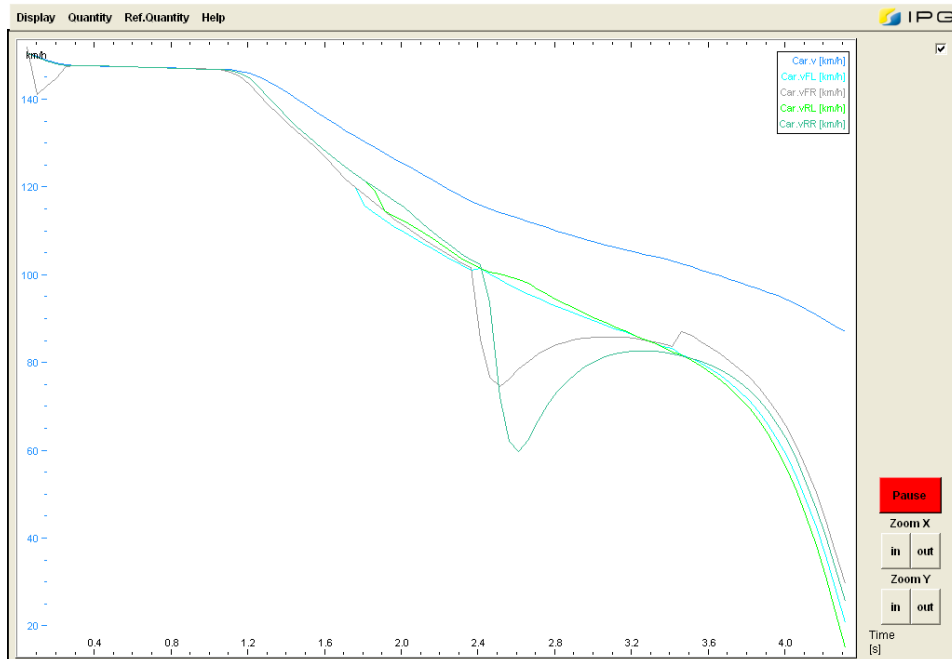
FIGURE 4.22: WHEEL & VEHICLE VELOCITIES (SCENARIO IV, STD-ABS, 50°)
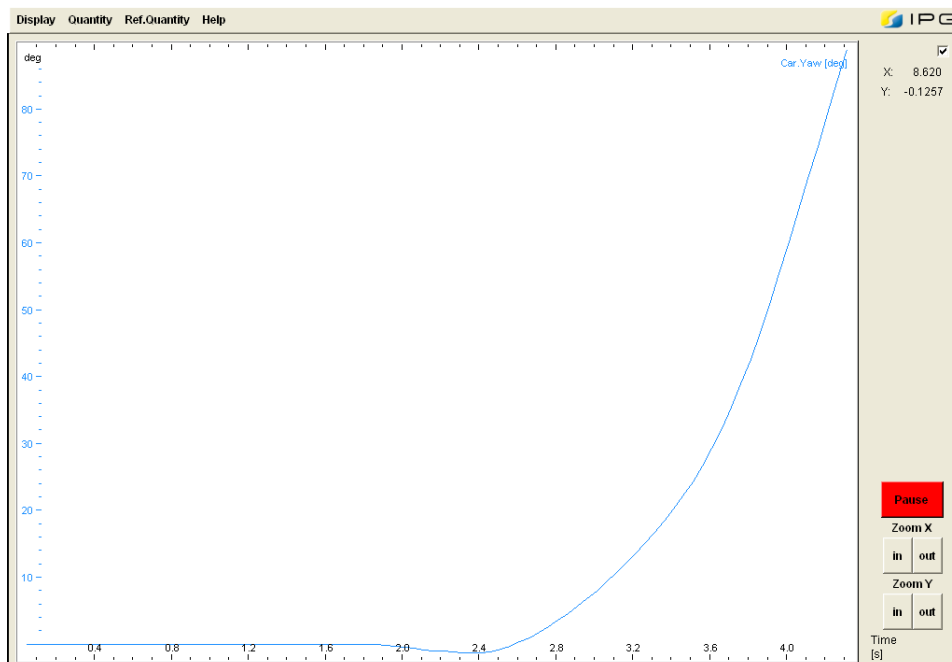

FIGURE 4.23: YAW ANGLE (SCENARIO IV, STD-ABS, 50°)

68

SMC-ABS:

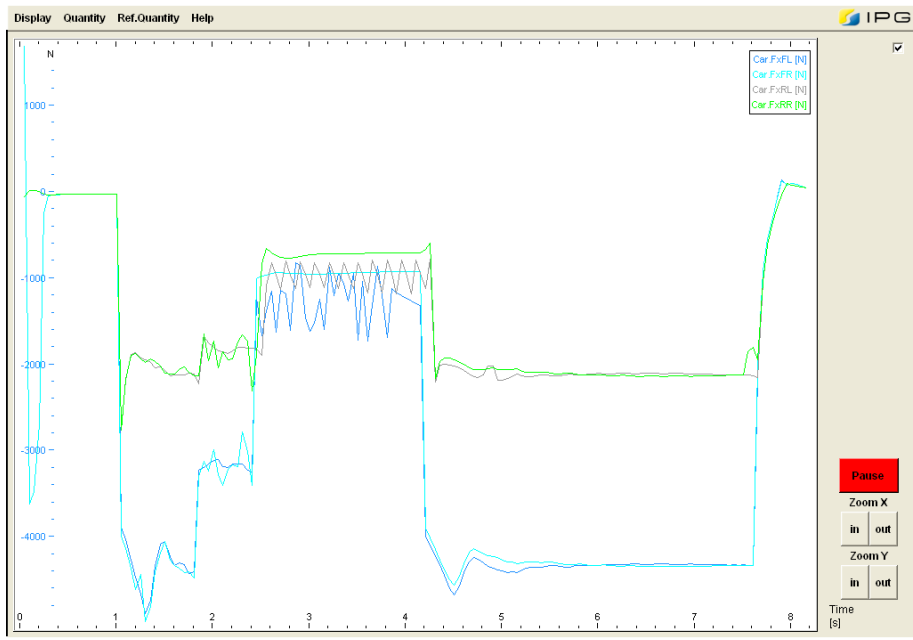The braking distance value : **289.18m**

FIGURE 4.24 FRICTION FORCES (SCENARIO IV, SMC-ABS, 50°)

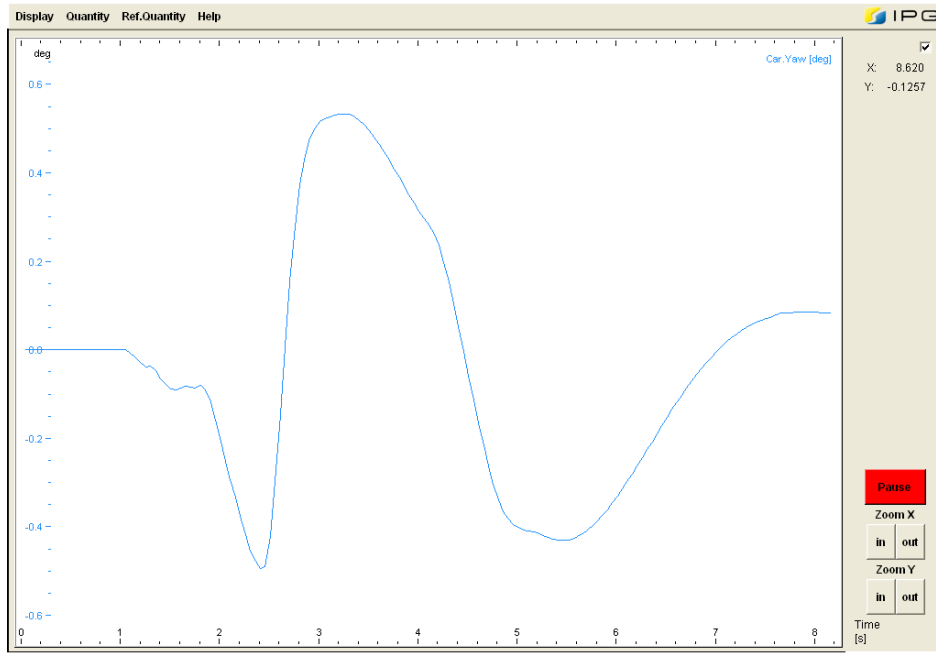FIGURE 4.25: WHEEL & VEHICLE VELOCITIES (SCENARIO IV, SMC-ABS, 50°)

FIGURE 4.26: YAW ANGLE (SCENARIO IV, SMC-ABS, 50°)

4.3 Conclusion

If we look at the results of the first two scenarios which are shown in Figures 4.-4. We can see that the SMC-ABS definitely does its job. The friction forces are maximized in both cases. The conventional ABS sticks to a fixed slip value which results in a longer brake distance. The difference between the distances are 9m and 15m respectively both which correspond to a 7% better performance.

However, when we look at the scenario III, the results are different. There is a huge difference between the braking distances. It is almost 73m. The conventional ABS seems to work much better. On the other hand the stability performances are the opposite. Maximum yaw angle reached during driving is 0.4° with SMC-ABS and the conventional one has a maximum of 8°. This scenario helps us to understand the trade-off between the stability and the braking distance. If the driver can handle the vehicle in spite of the continuous moment arising from the friction force difference the maximization of the friction forces will definitely the best choice. So, the solution of this problem lies in the

direct control of the yaw rate of the vehicle which leads us to electronic stability program (ESP).

The final scenario clearly shows us the trade-off between the brake distance and stability. The conventional ABS fails to maintain the stability of the vehicle even the driver has the maximum steer ability. And in the 50° limited steer ability case the vehicle with conventional ABS spins and leaves the road. On the other hand SMC-ABS, regardless of the steer ability limitation, provides very good handling and almost the same brake distance with conventional ABS.

Although we have seen that in the 3rd scenario SMC-ABS does not satisfy very much, the possibility of scenario 4 is much more than the scenario 3. In most of the cases the road surface is partially frozen or wet. As a result the overall performance of the SMC-ABS is, as expected, satisfactory.

The work carried out in this thesis can be considered as a complete ABS system and a basic stability control system which can be extended to a full stability control program.

Bibliography

Drakunov, S., Ozguner, U., Dix, P., & Asrafi, B. (1995). ABS Control Using Optimum Search via Sliding Modes. *IEEE Transactions On Control Systems Technology Vol 3 No 1* (pp. 79-85 IEEE TRANSACTIOWS OU CONTROL SYSTEMS IECHYOLOGY VO1 7 NO I , MARCH lY9S). IEEe.

Buckholtz, K. (2002). Reference Input Wheel Slip Tracking Using Sliding Mode Control. *SAE World Congress Detroit Michigan* .

Burckhardt, M. (1993). *Fahrwerktechnik: Radschlupf-Regelsysteme.* Würzburg: Vogel Verlag.

Freeman, R. (1995). *Robust slip control for a single wheel. Research Report CCEC 95-0403.* Santa Barbara.: University of California.

Jiang, F. (2000). *A novel approach to a class of antilock brake problems PhD Thesis.* Cleveland: Cleveland State University.

Jun, C. (. (1998). The study of ABS control system with different control methods. *In Proceedings of the 4th International Symposium on Advanced Vehicle Control*, (pp. 623-628). Vehicle Control, Nagoja, Japan.

Kiencke, U., & Nielsen, L. (2000). *Automotive Control Systems.* Verlag: Springer.

Ozguner, U., & Xu, R. (2005). Extremum Seeking via Sliding Mode with Two Surfaces.

SAE. (1992). *Anti-lock brake system review.Technical Report J2246.* Warrendale, PA: Society of Automotive Engineers.

Solyom, S., & Rantzer, A. (2002). Chapter ABS Control - A Design Model and Structure . In *Nonlinear and Hybrid Control in Automotive Applications* (pp. 85-96). Verlag: Springer.

Unsal, C., & Kachroo, P. (1999). Sliding Mode Measurement Feedback Control for Antilock Braking Systems. *IEEE TRANSACTIONS ON CONTROL SYSTEMS TECHNOLOGY, VOL. 7, NO. 2* (pp. 271-281). IEEE.

Utkin, V. (1999). *Sliding Mode Control in Electromechanical Systems.* CRC Press.

Utkin, V. (1992). *Sliding Modes in Control and Optimization.*

Utkin, V., & Chang, H. (2002). Sliding Mode Control on Electromechanical Systems. *Mathematical Problems in Engineering* (pp. 451-473). Taylor&Francis.

Yu, J. S. (1997). A robust adaptive wheel-slip controller for antilock brake system. *36th IEEE Conf. on Decision and Control* (pp. 2545-2546). San Diego: IEEE.